GEORGIA INSTITUTE OF TECHNOLOGY — OFFICE OF CONTRACT ADMINISTRATION

PROJECT ADMINISTRATION DATA SHEET

[X] ORIGINAL [ ] REVISION NO. ____

Project No. G-35-628 GTRI/~~GIT~~ DATE 4/22/83

Project Director: Dr. Franco Einaudi School/~~Lab~~ Geo. Sci.

Sponsor: National Science Foundation

Type Agreement: Grant No. ATM-8213784

Award Period: From 3/1/83 To ~~8/31/84~~ 9-30-86 4-30-87 (Performance) 11/30/84 (Reports)

Sponsor Amount: Total Estimated: $ 95,700 Funded: $ 95,700

Cost Sharing Amount: $ 2,500 Cost Sharing No: G-35-315

Title: An Investigation of the Interaction Between Turbulence and Propagating Internal Gravity Waves in the Planetary Boundary Layer

ADMINISTRATIVE DATA OCA Contact Frank H. Huff x-4820

1) Sponsor Technical Contact:

Dr. Jack Kornfield (Program Officer)
Associate Director for Meteorology
National Science Foundation
1800 G Street
Washington, D. C. 20550
Phone: (202) 357-7624

2) Sponsor Admin/Contractual Matters:

Lee A. Delterrera
National Science Foundation
1800 G. Street
Washington, D. C. 20550
Phone: (202) 357-9602

Defense Priority Rating: N/A

Military Security Classification: N/A
(or) Company/Industrial Proprietary: ____

RESTRICTIONS

See Attached NSF ** Supplemental Information Sheet for Additional Requirements.

Travel: Foreign travel must have prior approval – Contact OCA in each case. Domestic travel requires sponsor approval where total will exceed greater of $500 or 125% of approved proposal budget category.

Equipment: Title vests with Georgia Tech

COMMENTS:

* Includes usual six (6) month unfunded flexibility period.
Note that grant has scientific/technical approval for a total of three (3) years depending on availability of funds.

** Old NSF conditions apply because of March 1 effective date.

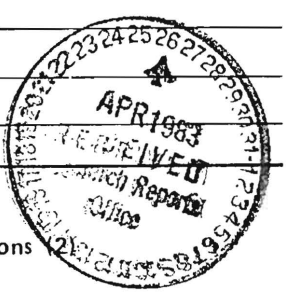

COPIES TO:

Research Administrative Network
Research Property Management
Accounting
Procurement/EES Supply Services
Research Security Services
Reports Coordinator (OCA)
GTRI
Library
Research Communications (2)
Project File
Other Einaudi
Other I. Newton

GEORGIA INSTITUTE OF TECHNOLOGY
OFFICE OF CONTRACT ADMINISTRATION

NOTICE OF PROJECT CLOSEOUT

No. 2 SR, 147

Closeout Notice Date 04/30/90

Project No. G-35-628 Center No. R5612-1A0

Project Director EINAUDI F School/Lab E & A SCI

Sponsor NATL SCIENCE FOUNDATION/GENERAL

Contract/Grant No. ATM-8213784 Contract Entity GTRC

Prime Contract No.

Title INVES INTERACTION BETWN TURBULENCE & PROPAGATION INTERNAL GRAVITY WAVES .

Effective Completion Date 870430 (Performance) 870731 (Reports)

Closeout Actions Required:	Y/N	Date Submitted
Final Invoice or Copy of Final Invoice	N	
Final Report of Inventions and/or Subcontracts	N	
Government Property Inventory & Related Certificate	N	
Classified Material Certificate	N	
Release and Assignment	N	
Other	N	

Comments

Subproject Under Main Project No.

Continues Project No.

Distribution Required:

Project Director	Y
Administrative Network Representative	Y
GTRI Accounting/Grants and Contracts	Y
Procurement/Supply Services	Y
Research Property Managment	Y
Research Security Services	N
Reports Coordinator (OCA)	N
GTRC	N
Project File	Y
Other	N
	N

Report on the work performed during the period March 1, 1983 - January 31, 1984 for the Grant

An Investigation of the Interaction Between Turbulence and Propagating Internal Gravity Waves in the Planetary Boundary Layer

The work performed during this time can be divided in three parts: installation of additional microbarographs at the Boulder Atmospheric Observatory (BAO) and development of related software; identification of atmospheric events which may be suitable for detailed analysis; theoretical analysis of the turbulence-gravity wave systems. A brief summary of the work performed in each of these areas follows.

a) Work performed at the BAO

The cables and sensors have been installed to provide three additional microbarograph stations at the BAO. The new system has been in operation since about October, 1983. The new data have been integrated into the existing data collection system.

Software is being developed to combine the data from the microbarograph stations at the BAO with those of he microbarograph stations in the Boulder Wind Network (BWN). This arrangement should increase substantially our capability to produce a climatology of gravity waves for this area.

b) Identification of atmospheric events

The following atmospheric events have been identified through a very preliminary screening. The meaning of one, two and three stars is as follows:

*Clear wave event with continuous wave train; a complete analysis is precluded by rapid frequency variation or incomplete data set.

**Good data for complete analysis. All instruments are working.

***Possible examples of propagating solitary waves.

Date of event	Comments
10/14/83	substantial K-H activity with 3 hours record
10/18/83	***
10/23/83	***
10/31/83	large transient wave
11/05/83	*
11/08/83	wave-turbulence event
11/16 and 17/83	good event, but no temperature data
12/12/83	large clear wave but with frequency change
12/13/83	***
12/16/83	*
12/17/83	wave-turbulence event
12/18 and 16/83	**
12/20/83	large amplitude nonlinear wave

12/22 and 23/83	substantial wave with changing frequency and amplitude
01/04/84	***
01/15/84	**
01/18 and 19/84	wave and turbulence event

The analysis of some of the double starred events is just starting.

c) Theoretical analysis

We have made progress in two directions. We have completed an analytical numerical analysis of the interaction between a gravity wave and turbulence in the presence of a critical level using a "1-1/2th order" scheme. The paper "Gravity wave turbulence interaction in the presence of a critical level" by F. Einaudi, J.J. Finnigan and D. Fua has been accepted in the Journal of Atmospheric Sciences.

We have also made progress in our attempt to extent the rapid distortion theory of turbulence behavior to the case in which the atmosphere is statically stable and the background velocity profile is arbitrary.

G-35-628

Report on the work performed during the period March 1, 1983 - February 28, 1985, for the Grant No. ATM-8213784

An Investigation of the Interaction Between Turbulence and Propagating Internal Gravity Waves in the Planetary Boundary Layer.

A brief summary of the work done during this time follows along the lines of the three main objectives of the proposal: A) To establish a climatology of gravity waves at the Boulder Atmospheric Observatory (BAO) site; B) To study the detailed dynamics of wave-turbulence interactions; C) To develop a numerical program to study the stability of a system which includes a height dependent eddy viscosity and conductivity and to extend rapid distortion models to include the treatment of an internal gravity wave.

A) On the climatology of gravity waves.

The cables have been installed to provide three additional microbarographs stations at the BAO. This was done during the first year of the grant and the new system has been in operation since about October, 1983. The software has been developed with the following objectives:

a) To transfer the gravity wave data on disk for archiving and plotting.

b) To develop a scheme able to combine a beamstearing program for the identification of the wave parameters with a program designed to compute various parameters along the tower. The capabilities of this combined program can be summarised as follows:

i) It calculates the rms values for the atmospheric pressure and the associated peaks, for a given pass band.

ii) It calculates the cross-correlation coefficient, azimuth and speed of the wave motion.

iii) It calculates the kinetic energy, Richardson number, Brunt-Vaisala frequency, wind gradient, etc. at the various instrumented heights along the tower.

The program has been applied for the detailed analysis of the entire period from March 15, 1984 to April 15, 1984. This analysis is almost complete and we hope to have a manuscript ready in the next few months, by Bedard, Einaudi and Finnigan. It will provide a climatology of gravity waves in the range 1-20 minutes and their relationship to minimum Richardson number, Brunt-Vaisala frequency and kinetic energy along the tower. I include a sample of the calculations performed, as Appendix A.

B) On the dynamics of wave-turbulence systems.

The paper "The Interaction Between an Internal Gravity Wave and Turbulence in the Stably-Stratified Nocturnal Boundary Layer" by Finnigan, Einaudi and Fua was completed in the early part of the grant and has now appeared in the Journal for the Atmospheric Sciences, 1984, 41, 2409.

We have made progress in our understanding of a wave-turbulence system in the earth boundary layer, by studying 6 new events which took place at the following times:

December 18, 1983: 2030 - 2110 MST

December 18, 1983: 2120 - 2200 MST

December 19, 1983: 2300 - 2350 MST

February 5, 1984: 0720 - 0810 MST

March 2, 1984: 0310 - 0400 MST

March 2, 1984: 0520 - 0550 MST

These events correspond to different values of stratification.

It is found that in the neutral and least stably stratified cases the transfer of energy from wave to turbulence is limited by an approximate quadrature relationship between the periodic part of the turbulent stresses and the wave rate of strain. In addition, in these cases, the temperature fluctuations are very small.

In the remaining cases, the phase difference between the periodic part of the turbulent stresses and the wave rate of strain is about $\pi/4$ and there is significant energy transfer with substantial reenforcement of the turbulent kinetic energy from the wave field. In all the latter cases, the distinguishing feature is the presence of a substantial fluctuating componènt of the temperature field.

The analysis suggests that the departure from quadrature is the result of periodicity in the stratification.

The above results are described in a very rough draft of the paper "Kinetic Energy Transfer Between Internal Gravity Waves and Turbulence" by J.J. Finnigan, which is enclosed as Appendix B.

C) Theoretical analysis.

We have completed the analytical-numerical analysis of the interaction between a gravity wave and turbulence in the presence of a critical level using a "$1^{1/2}$th order" scheme. The paper "Gravity Wave Turbulence Interaction in the Presence of a Critical Level" by F. Einaudi, J.J. Finnigan and D. Fua has appeared in the Journal of the Atmospheric Sciences, 1984, 41, 661.

The analytical-numerical analysis of the stability of a an horizontally homogeneous system in the presence of height dependent eddy diffusion coefficients for temperature and momentum has been completed. The paper "On the Effect of Dissipation on Shear Instabilities in the Atmospheric Boundary Layer" by D. Fua and F. Einaudi has appeared in the Journal of the Atmospheric Sciences, 1984, 41, 888.

We have also made progress in our attempt to extend the rapid distortion theory of turbulence to the case in which the atmosphere is statically stable and the background velocity profile is arbitrary. In fact we have obtained a final formal solution which involves the calculation of the Green function for the system and the numerical evaluation of a number of integrals. We are studying the feasibility of the numerical evaluation of these integrals which might require the use of the GRAY computer.

Brief outline of the work to be performed during the third year of the grant.

1) Besides completing the present analysis of the period March 15-April 15, 1984, we are planning a second observational period involving a larger network of absolute microbarographs. Five will be along an East-West line and are part of the Boulder wind network, one is at the tower and one will be added so as to have a distribution of sensors forming triangles of about 10 km in size. This network will allow us to extend our climatological study to much longer horizontal wavelengths and longer periods.

2) In addition to the completion of the analysis of the cases discussed in Appendix B, we intend to continue to assemble more properly

analyzed cases of wave-turbulence interactions.

Work will continue on the time interval of over 35 hours from at least 1500 MST on 18 December to past 0500 MST on 20 December, 1983, when waves appear to form a continuous train of non-linearly interacting Kelvin-Helmholtz.

3) A major effort will be made to complete the extension of the rapid distortion theory to the case of a stratified fluid in the presence of an arbitrary velocity profile.

3rd year

OMB No. 3145-0058
Exp. Date 12/31/85

SUMMARY PROPOSAL BUDGET

FOR NSF USE ONLY

ORGANIZATION	PROPOSAL NO.	DURATION (MONTHS) Proposed	Granted
GEORGIA TECH RESEARCH CORPORATION			
PRINCIPAL INVESTIGATOR/PROJECT DIRECTOR: Einaudi, Franco	AWARD NO.		

A. SENIOR PERSONNEL. PI/PD, Co-PI's, Faculty and Other Senior Associates (List each separately with title, A.6. show number in brackets)	NSF FUNDED PERSON-MOS. CAL.	ACAD	SUMR	FUNDS REQUESTED BY PROPOSER	FUNDS GRANTED BY NSF (IF DIFFERENT)
1. Franco Einaudi	3			$17,500	$
2. John J. Finnigan	3			12,100	
3.					
4.					
5. ( ) OTHERS (LIST INDIVIDUALLY ON BUDGET EXPLANATION PAGE)					
6. (2) TOTAL SENIOR PERSONNEL (1-5)	6			29,600	
B. OTHER PERSONNEL (SHOW NUMBERS IN BRACKETS)					
1. ( ) POST DOCTORAL ASSOCIATES					
2. ( ) OTHER PROFESSIONALS (TECHNICIAN, PROGRAMMER, ETC.)					
3. (1) GRADUATE STUDENTS 1/2				13,500	
4. (1) UNDERGRADUATE STUDENTS part time				1,000	
5. ( ) SECRETARIAL CLERICAL 1 mo. time				1,210	
6. ( ) OTHER					
TOTAL SALARIES AND WAGES (A+B)				45,310	
C. FRINGE BENEFITS (IF CHARGED AS DIRECT COSTS) 21.2% of A.1 & B.5+5.75% of A.2				4,662	
TOTAL SALARIES, WAGES AND FRINGE BENEFITS (A+B+C)				49,972	
D. PERMANENT EQUIPMENT (LIST ITEM AND DOLLAR AMOUNT FOR EACH ITEM EXCEEDING $1,000:) This amount includes trips to Boulder, CO for P.I.'s and graduate student.					
TOTAL PERMANENT EQUIPMENT					
E. TRAVEL 1. DOMESTIC (INCL. CANADA AND U.S. POSSESSIONS)				3,000	
2. FOREIGN					
F. PARTICIPANT SUPPORT COSTS					
1. STIPENDS $					
2. TRAVEL					
3. SUBSISTENCE					
4. OTHER					
TOTAL PARTICIPANT COSTS					
G. OTHER DIRECT COSTS					
1. MATERIALS AND SUPPLIES				500	
2. PUBLICATION COSTS/PAGE CHARGES				2,000	
3. CONSULTANT SERVICES					
4. COMPUTER (ADPE) SERVICES on Ga.Tech CYBER 170/730 at DCAA-approved rates				1,000	
5. SUBCONTRACTS WAVE PROPAGATION LABORATORY OF NOAA				5,000	
6. OTHER					
TOTAL OTHER DIRECT COSTS				8,500	
H. TOTAL DIRECT COSTS (A THROUGH G)				61,472	
I. INDIRECT COSTS (SPECIFY) overhead of 64.2% MTDC includes the first $5,000 for subcontract to NOAA for 1st year only (overhead is not applied to subcontract for this budget)					
TOTAL INDIRECT COSTS				36,255	
J. TOTAL DIRECT AND INDIRECT COSTS (H + I)				97,727	
K. RESIDUAL FUNDS (IF FOR FURTHER SUPPORT OF CURRENT PROJECTS GPM 252 AND 253)					
L. AMOUNT OF THIS REQUEST (J) OR (J MINUS K)				$97,727	$

PI/PD TYPED NAME & SIGNATURE*	DATE	FOR NSF USE ONLY
Franco Einaudi	3/15/85	INDIRECT COST RATE VERIFICATION
INST. REP TYPED NAME & SIGNATURE*	DATE	Date Checked / Date of Rate Sheet / Initials - DGC / Program
Lynn Boyd	3/21/85	

Current support and pending applications

Dr. Einaudi and Dr. Finnigan have no current support from other grants or contracts.

Appendix A: Samples of the climatological study carried out during the time interval March 15 - April 15, 1984.

Fig. A1: Three dimensional plot with the frequency of occurrence on the vertical (height of towers), vs. cross-correlation coefficient and time of day. The analysis is carried out over 4 separate ranges of wave periods (which we call STOUTS); STOUT 1, 2, 3 and 4 refer to the period ranges 1-3 minutes, 3-5 minutes, 5-10 minutes, 10-20 minutes, respectively.

Fig. A2: Histogram for cross-correlation, i.e., frequency of occurrence of events with a given value of the cross-correlation coefficient.

Fig. A3. Three-dimensional plots for rms power vs. time, for STOUT 1 and for ranges of the correlation coefficient of 0-1, .5-1, 0-.5, and .7-1, respectively.

Fig. A4: Three-dimensional plot of the frequency of occurrence of the minimum value of the Richardson number along the tower vs. time of day for STOUT 1. The values of the corresponding ranges of correlation coefficients of the waves are 0-1, .5-1, 0-.5, respectively.

Fig. A5: Histogram for the minimum value of the Richardson number along the tower, for STOUT 1.

Fig. A6: Histogram for the Brunt-Vaisala frequency squared calculated where the Richardson number reaches its minimum value along the tower, for STOUT 1.

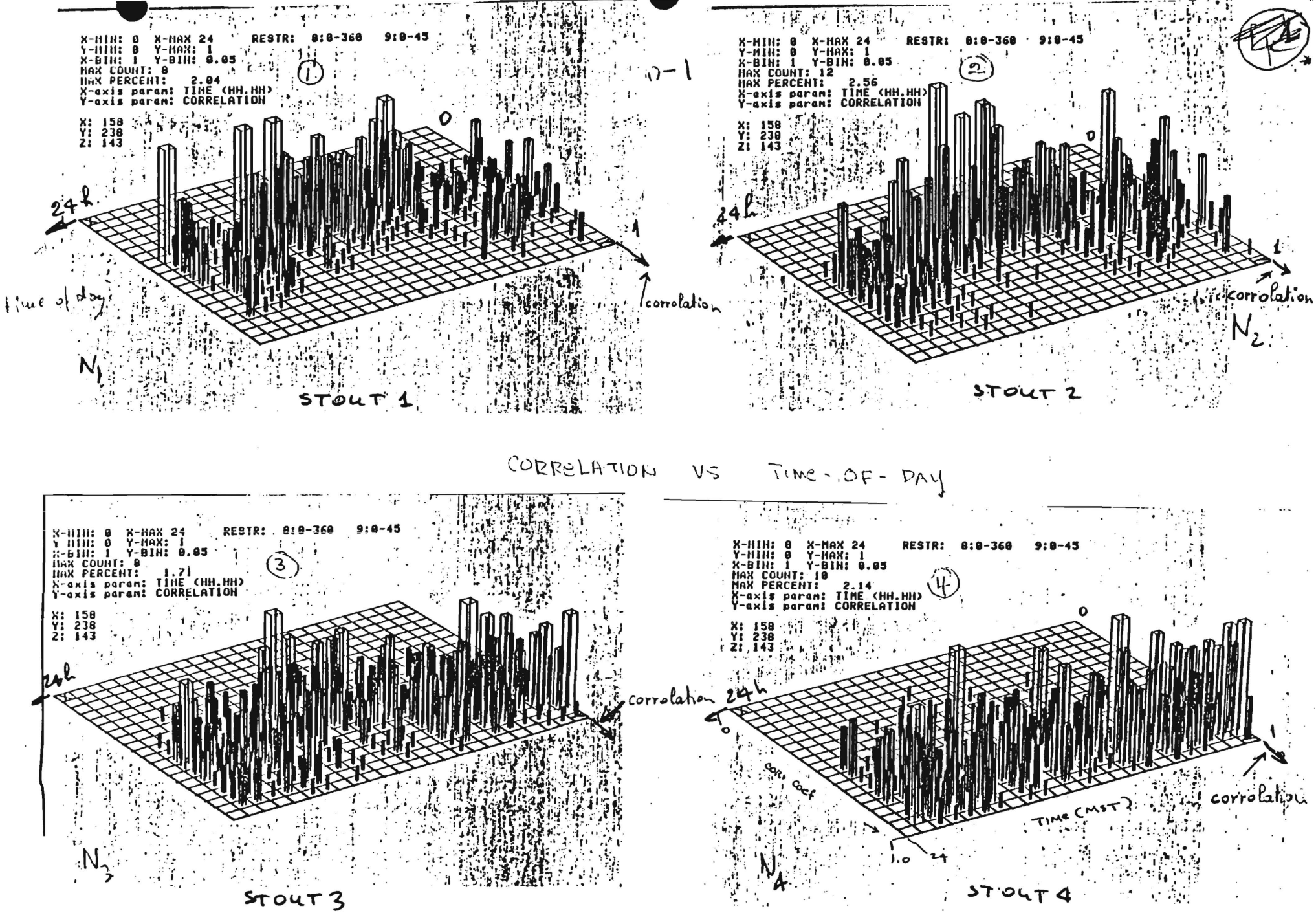
X-MIN: 0 X-MAX 24 RESTR: 0:0-360 9:0-45
Y-MIN: 0 Y-MAX: 1
X-BIN: 1 Y-BIN: 0.05
MAX COUNT: 0
MAX PERCENT: 2.04
X-axis param: TIME (HH.MM)
Y-axis param: CORRELATION
X: 158
Y: 238
Z: 143
1
0
24h
1
time of day
correlation
N1
STOUT 1
X-MIN: 0 X-MAX 24 RESTR: 0:0-360 9:0-45
Y-MIN: 0 Y-MAX: 1
X-BIN: 1 Y-BIN: 0.05
MAX COUNT: 12
MAX PERCENT: 2.56
X-axis param: TIME (HH.MM)
Y-axis param: CORRELATION
X: 158
Y: 238
Z: 143
2
0
24h
1
1
correlation
N2
STOUT 2
CORRELATION VS TIME-OF-DAY
X-MIN: 0 X-MAX 24 RESTR: 0:0-360 9:0-45
Y-MIN: 0 Y-MAX: 1
X-BIN: 1 Y-BIN: 0.05
MAX COUNT: 0
MAX PERCENT: 1.71
X-axis param: TIME (HH.MM)
Y-axis param: CORRELATION
X: 158
Y: 238
Z: 143
3
24h
correlation
N3
STOUT 3
X-MIN: 0 X-MAX 24 RESTR: 0:0-360 9:0-45
Y-MIN: 0 Y-MAX: 1
X-BIN: 1 Y-BIN: 0.05
MAX COUNT: 10
MAX PERCENT: 2.14
X-axis param: TIME (HH.MM)
Y-axis param: CORRELATION
X: 158
Y: 238
Z: 143
4
0
24h
1
corr. coef
TIME (MST)
correlation
1.0
24
N4
STOUT 4

FIG A.1

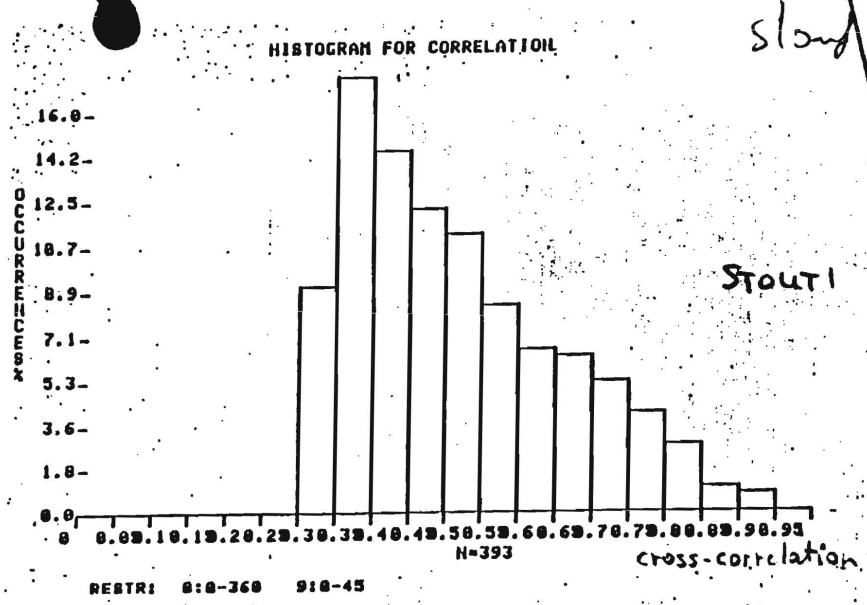

Slant 1

STOUT 1

2a

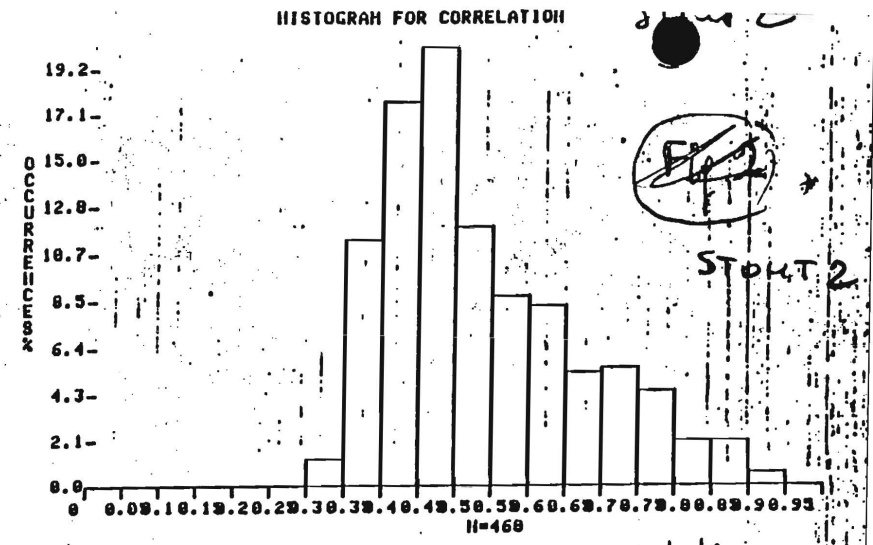

STOUT 2

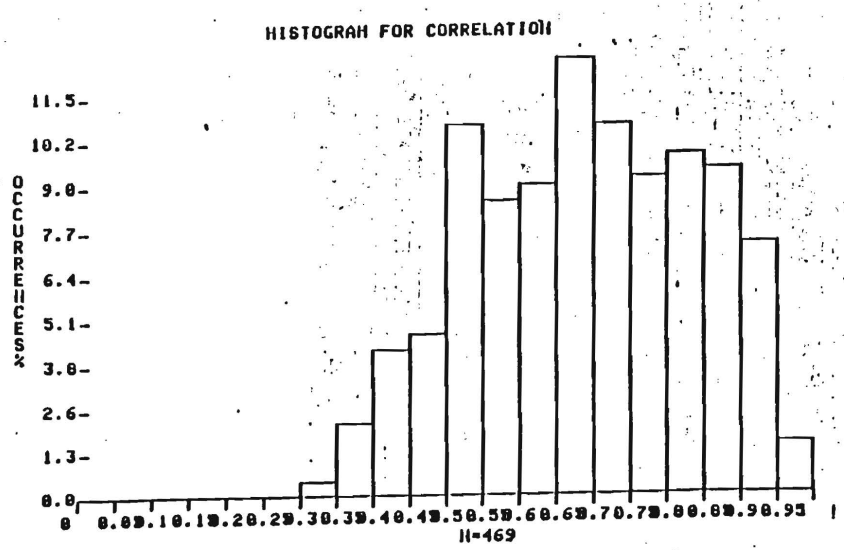

Slant 3

STOUT 3

cross-correlation

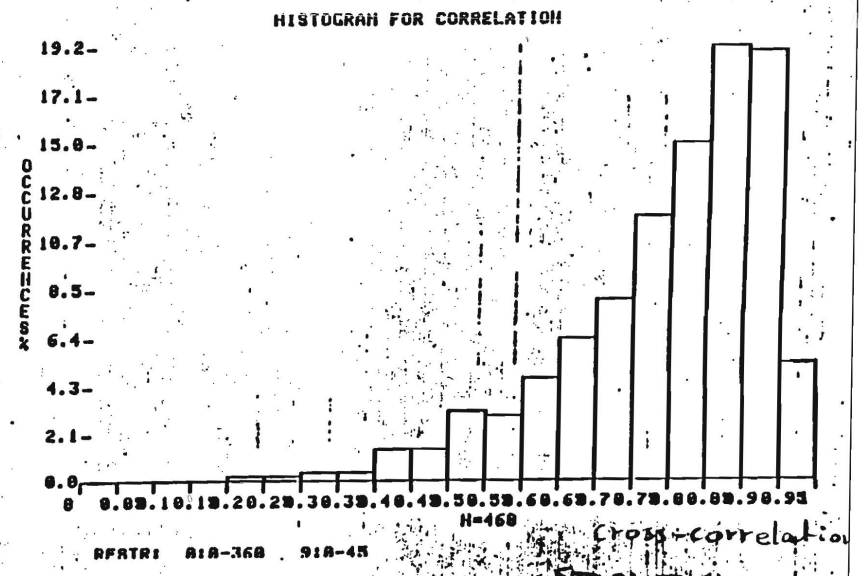

Slant 4

STOUT 4

FIG. A.2

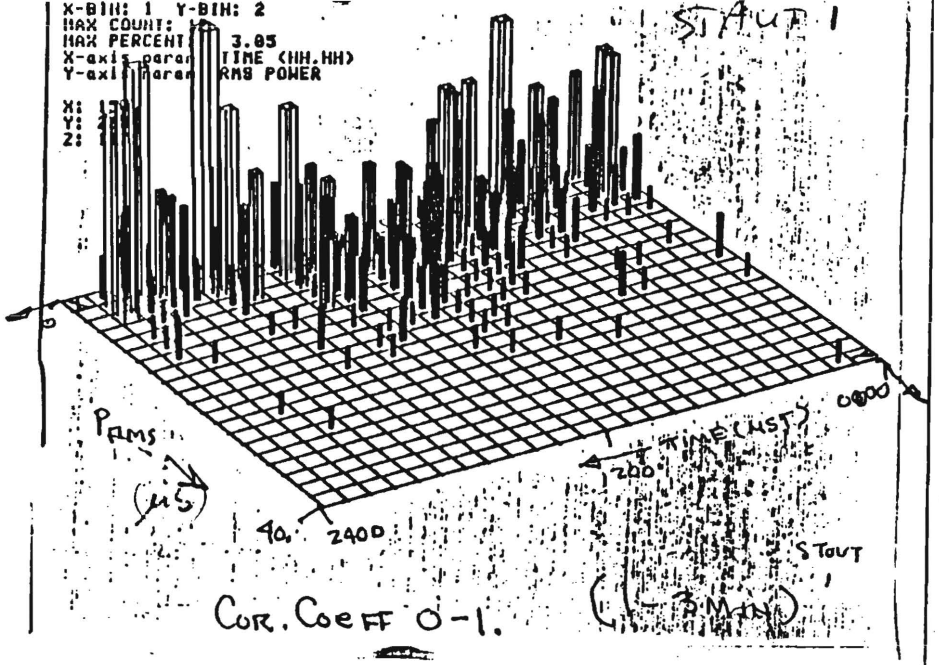

COR. COEFF 0-1.

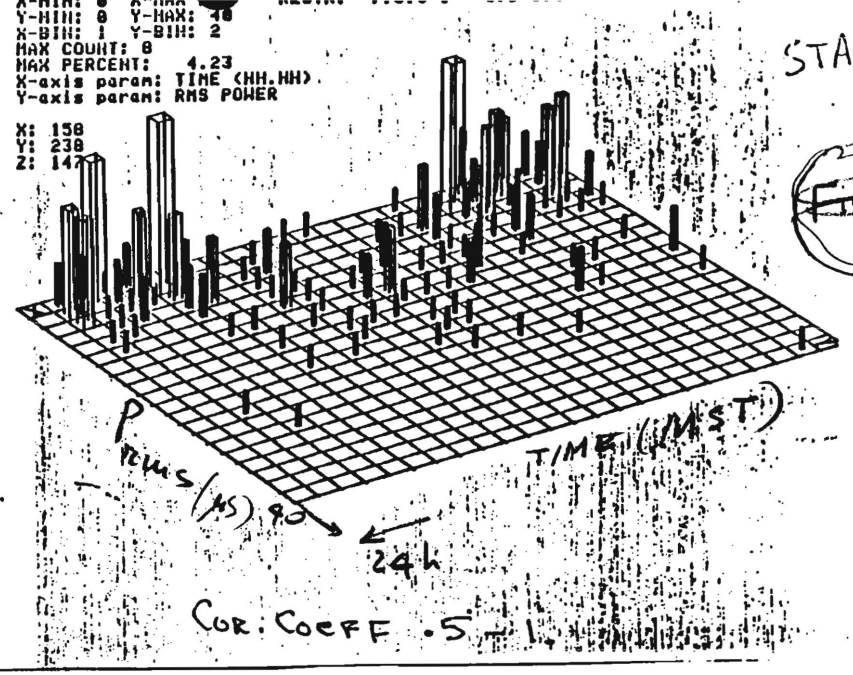

COR. COEFF .5-1.

(1-3 MIN) RMS Pressure vs Time of Day.

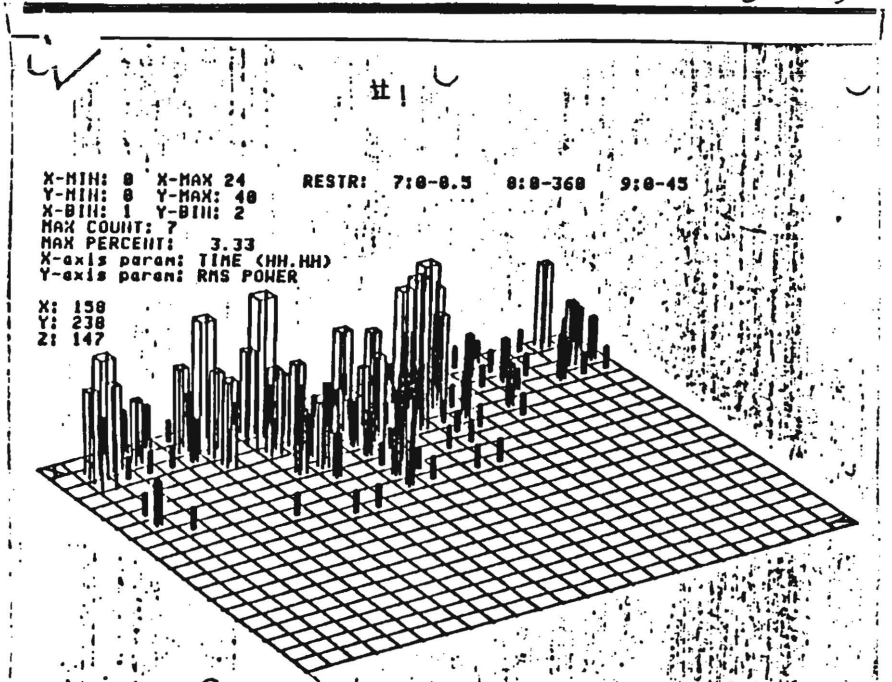

COR. COEFF 0-.5

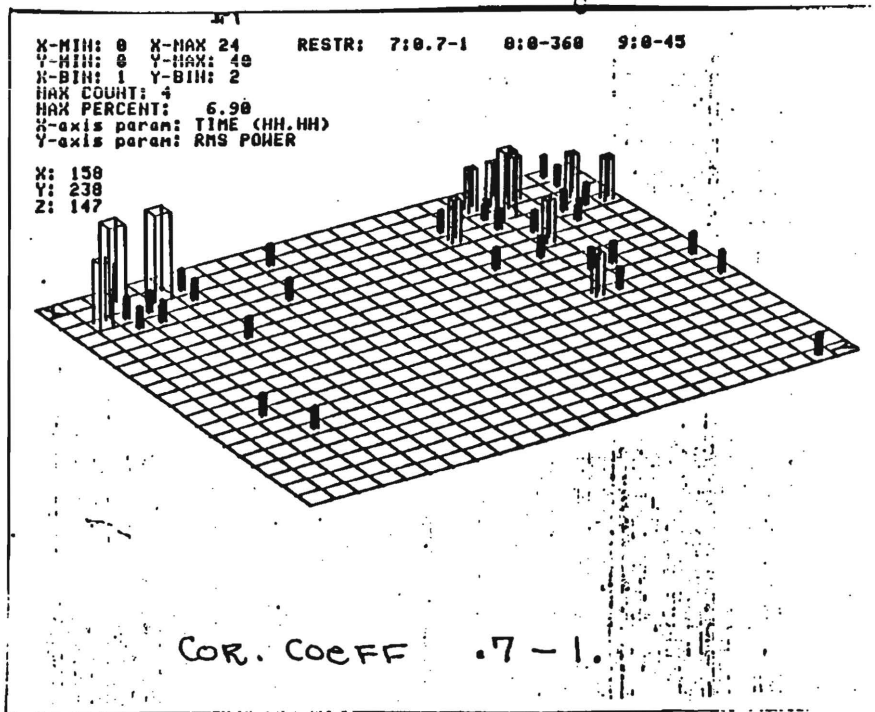

COR. COEFF .7-1.

FIG. A.3

Fig. 1

STOUT 1 sort for corr. coef.

R_i vs Time

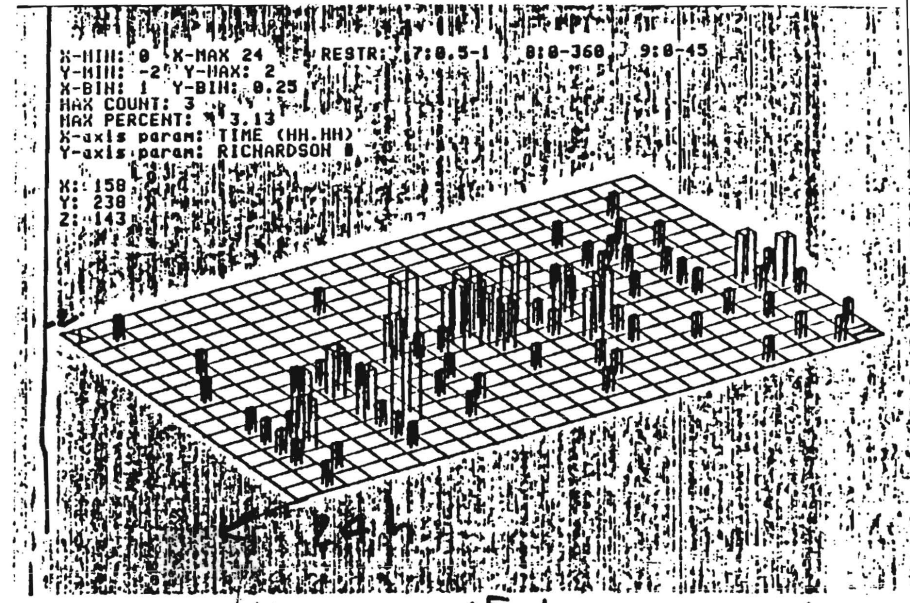

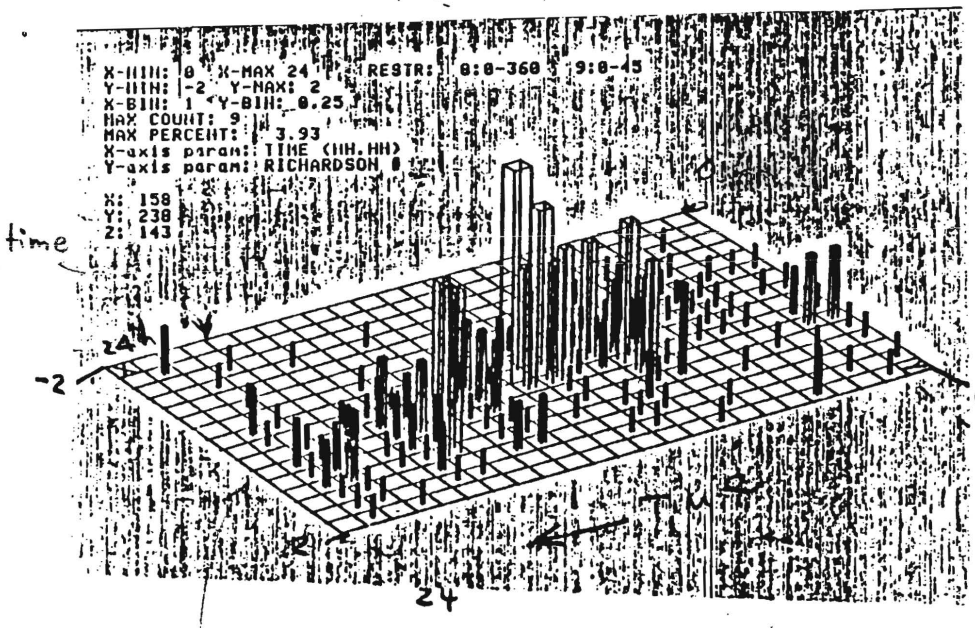

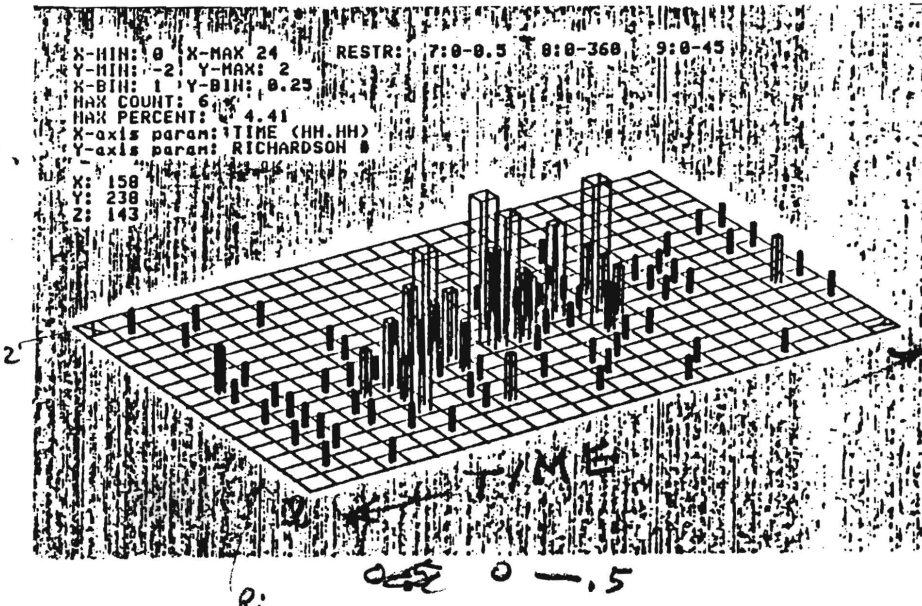

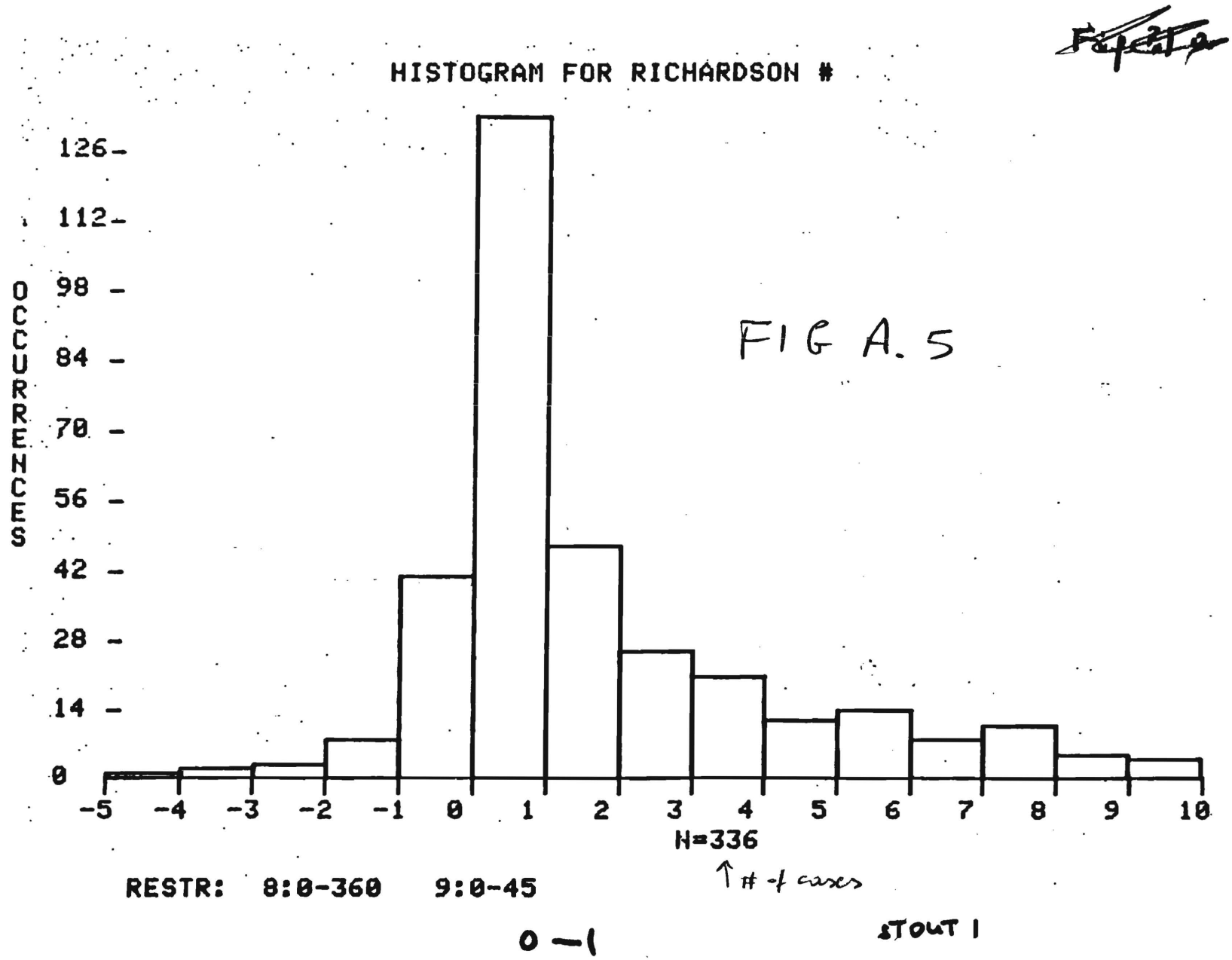
HISTOGRAM FOR RICHARDSON #
OCCURRENCES
126
112
98
84
70
56
42
28
14
0
-5 -4 -3 -2 -1 0 1 2 3 4 5 6 7 8 9 10
N=336
↑ # of cases
RESTR: 8:0-360 9:0-45
0 — 1
STOUT 1

FIG A.5

Figure a

STOUT1

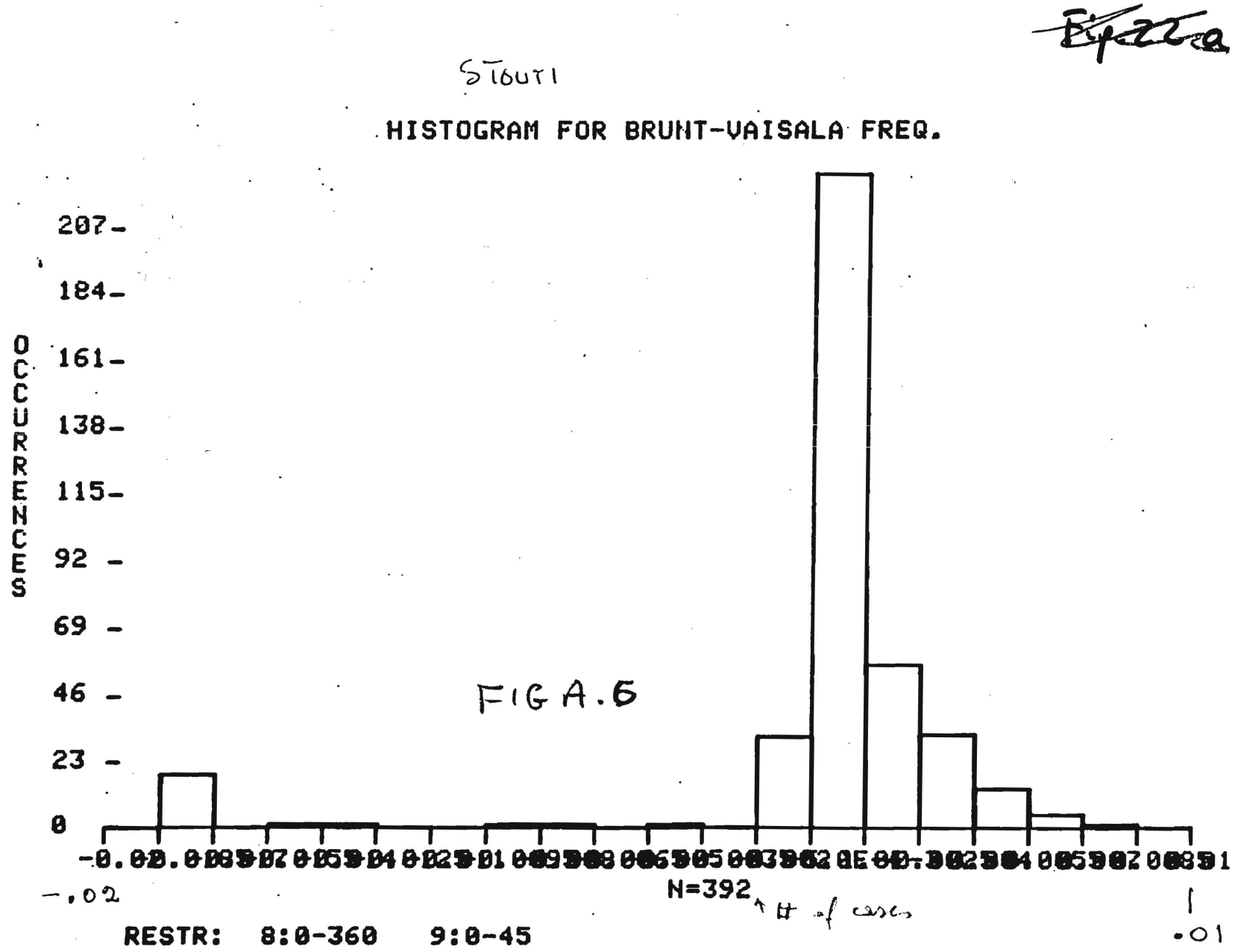

FIG A.6

Δ = .015

# of cases

G-35-628

APPENDIX VII

SCIENCE FOUNDATION
ington, D.C. 20550

FINAL PROJECT REPORT
NSF FORM 98A

PLEASE READ INSTRUCTIONS ON REVERSE BEFORE COMPLETING

PART I—PROJECT IDENTIFICATION INFORMATION

and Address	2. NSF Program	3. NSF Award Number
a Institute of Technology a, GA	ATM	ATM-8213784
	4. Award Period From To	5. Cumulative Award Amount

tle An Investigation of the Interaction Between Turbulence and Propagating Internal Gravity Waves in the Planetary Boundary Layer

PART II—SUMMARY OF COMPLETED PROJECT *(FOR PUBLIC USE)*

main objectives of the proposal were:

To establish a climatology of gravity waves at the Boulder Atmospheric Observatory (BAO) site,
To study the detailed dynamics of wave-turbulence interactions,
To study the effect of eddy viscosity and conductivity on the generation of gravity waves by sheer,
To extend rapid distortion models to include an arbitrary stratification and wind structure.

esults obtained on each item are briefly summarized below:

<u>On the climatology of gravity waves</u>

activities in this area have resulted in two publications. The main one (Einaudi, Bedard, and igan, 1989) represents the most comprehensive climatological study to date of gravity waves in the e of periods from 1 to 20 min, using BAO data. The study demonstrated that at these periods the sphere displays a highly coherent structure most of the time. During the interval from 0800 to 1800 coherent motions with cross-correlation coefficients larger than 0.5 are present about 25% of the for periods between 1 and 5 min and more than 80% of the time for periods between 10 and 20 min. e remaining hours of the day, the percentages rise to more than 40% and 95% of the time, ctively. The results have important implications on the behavior of the atmospheric boundary layer ts parameterization.

ond paper (Canavero and Einaudi, 1987) analyzes the temporal and spatial behavior of atmospheric ure data using a 60-day record obtained during the Alpine Experiment (ALPEX) which took place in . The study reveals that pressure records are intrinsically nonstationary and that the concept of rsality for atmospheric spectra may be a valid one, but that it must be recognized that averages over temporal or spatial data sets may produce results that mask the underlying physical processes. The also describes quantitatively the substantial effect of topography, particularly for periods below 40

PART III—TECHNICAL INFORMATION *(FOR PROGRAM MANAGEMENT USES)*

ITEM *(Check appropriate blocks)*	NONE	ATTACHED	PREVIOUSLY FURNISHED	TO BE FURNISHED SEPARATELY TO PROGRAM	
				Check (✓)	Approx. Date
cts of Theses					
ation Citations					
n Scientific Collaborators					
ation on Inventions					
ical Description of Project and Results					
(specify)					

I Investigator/Project Director Name *(Typed)*	3. Principal Investigator/Project Director Signature	4. Date

(1-87) Supersedes All Previous Editions

Form Approved OMB No. 3145-0058

B) On the dynamics of wave turbulence systems

Four papers were written on the interaction between waves and turbulence in the atmosphere. A theoretical one (Einaudi, Finnigan, and Fua, 1984) which analyzes the interactions between an interval gravity wave and the wave-induced turbulence, in the presence of a critical level. Using << 1 1/2 th order>> scheme, we show that a positive feedback can be established between the wave and the wave-induced turbulence, resulting in the wave growing at a faster rate than the one predicted by linear theory.

A second paper describes an aircraft turbulence-atmospheric gravity wave event which occurred over the Continental Divide. We show that the observed waves correspond to the unstable modes of the jet stream and that the position of the aircraft-reported turbulence coincides with the critical levels of the waves. This paper provides further evidence for the close relationship between waves and turbulence.

The following two papers complete a series of studies by the P.I. of the grant on wave-turbulence interactions using the BAO data. Finnigan (1988) analyzes eight-wave-turbulence events of different stability and shows that the only mechanism transferring energy between wave and turbulent fields is the work done by the periodic part of the turbulent stress against the wave rate of strain. When these components are $\pi/2$ out of phase, the net energy transfer is zero. Periodicity in the stratification changes the phase angle and leads to strong energy transfer from wave to turbulence.

Two events in the presence of strong stratification were analyzed by Einaudi and Finnigan (1991). Analysis of the budgets of wave heat flux and temperature variance revealed the essential role of wave-turbulence interaction in maintaining a large amplitude temperature wave and countergradient wave heat flux. A comparison with earlier near-neutral and stable cases analyzed in comparable detail by the P.I.'s suggests that the countergradient heat fluxes maintained by non-linear wave-turbulence interaction and the destabilization of the boundary layer by the wave so that both wave and turbulence may extract kinetic energy from the background state may be generic features of the boundary layer. This hypothesis provides a general mechanism for maintenance of turbulence by waves in strongly stratified boundary layers.

C) On the effect of eddy viscosity and conductivity on atmospheric stability

An analytical-numerical analysis of the stability of an horizontally homogeneous system in the presence of height dependent eddy diffusion coefficients for temperature and momentum was presented in a paper by Fua and Einaudi (1984). We show that vertical gradients of the eddy coefficients substantially affect the phase velocities, growth rates, and vertical structure of the gravity wave and are responsible for the appearance of some counter-gradient heat fluxes and Reynolds stresses.

D) On the extension of rapid distortion theory

The analytical formulation of the extension of rapid distortion to the case of the arbitrary wind and temperature profiles was completed for a horizontally homogeneous system. However, the numerical model needed to deal with actual cases and to derive quantitative results was not completed. The P.I.'s are disappointed on the progress on this topic and are planning to complete this area of research at a future date.

E) Additional publications

Two additional research papers were in part supported by this grant. The papers by Einaudi et al., 1987, and Ferretti et al., 1988, to deal with cases of interactions of gravity waves and convection. While marginal with respect to the original objective of the grant, they contribute to our understanding of the role of gravity waves on mesoscale dynamics.

Publications Supported in Part by the NSF Grant:

Bedard, A. J., F. Canavero, and F. Einaudi, 1986: Atmospheric Gravity Waves and Aircraft Turbulence Encounters. *J. Atmos. Sci.*, **43**, 2838-2844.

Canavero, F. G. , and F. Einaudi, 1987: Time and Space Variability of Spectral Estimates of Atmospheric Pressure. *J. Atmos. Sci.*, **44**, 1589-1604.

Einaudi, F., J. J. Finnigan and D. Fua, 1984: Gravity Wave Turbulence Interaction in the Presence of a Critical Level. *J. Atmos. Sci.*, **41**, 661-667.

Einaudi, R., W. L. Clark, D. Fua, J. L. Green, and T. E. VanZandt, 1987: Gravity Waves and Convection in Colorado during July 1983. *J. Atmos. Sci.*, **44**, 1534-1553.

Einaudi, F., A. J. Bedard, and J. J. Finnigan, 1989: A Climatology of Gravity Waves and Other Coherent Disturbances at the Boulder Atmospheric Observatory during March-April 1984. *J. Atmos. Sci.*, **46**, 303-329.

Einaudi, F., and J. J. Finnigan, 1991: Wave-turbulence Dynamics in the Stably Stratified Boundary Layer. *J. Atmos. Sci.* (submitted).

Ferretti, R., F. Einaudi, and L. U. Uccellini, 1988: Wave Disturbances Associated with the Red River Valley Severe Weather Outbreak of 10-11 April 1979. *Meteorol. Atmos. Phys.*, **39**, 132-168.

Finnigan, J. J., 1988: Kinetic Energy Transfer between Internal Gravity Waves and Turbulence. *J. Atmos. Sci.*, **45**, 486-505.

Fua, D. and F. Einaudi, 1984: On the Effect of Dissipation on Shear Instabilities in the Stable Atmospheric Boundary Layer. *J. Atmos. Sci.*, **41**, 888-900.

Wave-Turbulence Dynamics in the Stably Stratified Boundary Layer

F. EINAUDI

Laboratory of Atmospheres, NASA/Goddard Space Flight Centre, Greenbelt, Maryland

and

J.J. FINNIGAN

CSIRO Centre for Environmental Mechanics, Canberra, Australia

(Manuscript received , in final form)

ABSTRACT

New data obtained at the Boulder atmospheric observatory (BAO) has been compared with a linear stability analysis of the background atmospheric state as measured by rawinsonde ascents. Reasonable agreement was obtained between the linear eigensolutions scaled by measured pressure at the base of the BAO tower and good agreement between the gross wave parameters such as wave length, period and vector phase velocity.

An investigation of the wave kinetic energy budget revealed that buoyant production of wave energy was a significant gain despite the strong stability ($R_i \geq 5$). Further analysis of the budgets of wave heat flux and temperature variance revealed the essential role of wave-turbulence interaction in maintaining a large amplitude temperature wave and countergradient wave heat flux. A consideration of the turbulent kinetic

energy budget showed many of the features of the wave budget including buoyant production through the countergradient heat flux.

A comparison with earlier near-neutral and stable cases analyzed in comparable detail suggests that these features - countergradient heat fluxes maintained by non-linear wave-turbulence interaction and the destabilization of the boundary layer by the wave so that both wave and turbulence may extract kinetic energy from the background state - may be generic features of such situations. This hypothesis provides a general mechanism for maintenance of turbulence by waves in strongly stratified boundary layers and emphasizes that the time-mean Richardson number is an irrelevant parameter at such times.

1. Introduction

Over the last one and a half decades, many experimental studies of the behaviour of gravity waves in the boundary layer have appeared in the literature. As representative examples we may cite Kjelaas et al., 1974; Caughey and Readings, 1975; Lalas and Einaudi, 1976; Nai-Ping et al., 1983; Hunt et al., 1983; Rees and Mobbs, 1988. However, very few of these have included the explicit separation of wave, turbulence, and mean field necessary for a complete treatment of wave-turbulence interaction. This paper is the latest in a series using data gathered at the Boulder Atmospheric Observatory (BAO), whose unique facilities permit this essential decomposition.

Einaudi and Finnigan (1981) and Finnigan and Einaudi (1981) carried out a stability analysis and made a detailed study of the various wave and turbulence budgets for one, marginally stable, event in an atmospheric boundary layer (ABL). Finnigan et al. (1984) produced a similar analysis for two more cases in a stable ABL. These, however, were characterized by substantial time variability and wave-wave interaction. Finnigan (1988) analyzed six more events of varying degrees of stability with the main objective of studying the phase relations between the periodic, wave induced component of the turbulent Reynolds stresses and the wave strain rates. This did not require the analysis of the linear stability of the system or of all the wave and turbulence budgets. In the present paper, two further events are analyzed in the same detail as the earlier cases making a total of eleven, spanning a stability range from near neutral to strongly stratified.

A prerequisite of the triple decomposition (mean-wave-turbulent fields) is the presence of a well defined wave of fixed frequency for a significant period of time. Typically, ten wave periods are required to perform a successful phase average, the technique used to separate wave and turbulence. Such events form a small subset of the total number of wave

events that occur. The unique advantage of the BAO is that continuous records of acoustic sounder facsimile and microbarograph output are available, extending over more than ten years. This allows events that permit this detailed analysis to be distinguished from the much larger number that, while we have no reason to believe differ in their dynamics, cannot be analyzed in this way.

The similarities in various mechanisms governing energy exchange that have emerged from these eleven events allow us now to draw some general conclusions about the role played by externally generated internal gravity waves in the stable boundary layer. By "externally generated" we mean waves whose critical levels reside on low level jets or shear layers above the turbulent region, although such critical levels can indeed be very close to the boundary layer and there is no reason to believe in principle that they are excluded from the turbulent layer. However, the theoretical work of Einaudi et al. (1984) suggests that waves with critical levels within the turbulent layer are likely to have very large growth or decay rates, which would disqualify them from the kind of analysis we conduct.

A particularly important conclusion that was first advanced in Finnigan et al. (1984), but which we now affirm with more confidence is that on flat ground with an essentially steady background state, gravity waves are necessary for the initiation and maintenance of turbulence during times of light winds and large, time-mean Richardson Number. The particular mechanisms involved include a periodic destabilizing of portions of the boundary layer by the wave and a specific nonlinear behaviour of the wave itself, that requires the presence of some turbulence. The behavior of the wave, therefore, departs considerably from that predicted by linear theory, even though the latter explains some of the wave's characteristics quite well.

Our belief in the universality of those mechanisms is strengthened by two further pieces of evidence. The first is the ubiquitous occurrence of

large scale coherent motions (waves) in the boundary layer during nighttime stable conditions. This is immediately apparent in an inspection of microbarograph records from the BAO and was quantified in the study of one months contiguous data by Einaudi et al. (1989). They found short period waves (1-5 min.) during 40% of the night during mid-March to mid-April, while longer periods (10-20 min.) were present 95% of the time. Basing his comments on European data, Bull (personal communication) suggests that these estimates might represent lower limits. Waves in the shorter period range are particularly well suited to interact with boundary layer turbulence since their frequencies and those of the energy containing range of turbulent eddies overlap. Clearly the events that we suggest trigger nocturnal stable layer turbulence are present in sufficient quantity to account for the observations of this phenomenon.

The second piece of evidence is the widespread observation of counter-gradient heat fluxes in nocturnal stable boundary layers (Finnigan et al. 1984; Li et al. 1983, Hunt et al. 1983). This, we intend to show, is a diagnostic of wave-generated stable layer turbulence. Other general features of high Richardson Number turbulent boundary layers such as their intermittency and the unique character of their velocity spectra are reviewed in Finnigan et al. (1984).

This paper begins by presenting a detailed analysis of one new case and a more cursory treatment of a second. Although the features of wave-turbulence dynamics revealed are not new, they offer valuable confirmation of earlier studies and indeed increase the number of events studied in this degree of detail from 3 to 5. Furthermore, the two new cases presented here are the first to combine strong stratification and near stationarity in the wave dynamics. The other stable cases studied in the same detail (Finnigan et al. 1984) are strongly nonstationary.

The analysis will be divided into two parts: firstly, a comparison between BAO data and a linear stability analysis of the whole troposphere

(up to 13 km) using data obtained from rawinsonde ascents at nearby Denver Airport; secondly, a discussion of the coupled kinetic energy budgets of wave and turbulence, which will include, necessarily, the budgets of wave heat flux and temperature variance. In each section, after presenting the new data, a comparison with previous results will be essayed. Finally, some general conclusions will be drawn. Throughout this paper, we refrain, in the interest of brevity, from detailed discussions of the technical points that arise when phase averaging is applied to real data. These are treated at length in Finnigan et al. (1984) and Finnigan (1988).

2. Instrumentation

The data used in this paper were obtained at the Boulder Atmospheric Observatory (BAO) in Erie, Colorado. The facility is fully described in Kaimal and Gaynor (1983) and we mention here only essential information. The instruments that provided data for this study were:

1. Fast response instruments-sonic anemometers and Platinum resistance thermometers-located at eight levels (10 m, 22 m, 50 m, 100 m, 200 m, 250 m, 300 m) along the 300 m high tower. They were sampled at 10 Hz after low-pass filtering at 5 Hz to avoid aliasing in spectral computations.
2. Slow response instruments - quartz thermometers, dew point hygrometers, and three-component Gill anemometers - located at the same levels along the tower and sampled at 1 Hz.
3. Eight sensitive microbarographs deployed around the tower (see Fig. 1). They too were sampled at 1 Hz.
4. A monostatic single beam acoustic sounder located near microbarograph number 70 at the bottom of the tower.

Further discussion of the characteristics of the data and their storage can

be found in Finnigan et al. (1984) and Finnigan (1988).

3. The equations of motion and the method of analysis

The velocity u_i, the density ρ, the temperature T, and the potential temperature θ satisfy the equations of conservation of momentum, mass, and energy which can be written as follows:

$$\rho\frac{du_i}{dt} + \frac{\partial p}{\partial x_i} + g\rho\delta_{i3} = \mu\frac{\partial^2 u_i}{\partial x_j \partial x_j} , \quad i = 1,2,3 \tag{1}$$

$$\frac{d\rho}{dt} + \rho\frac{\partial u_i}{\partial x_i} = 0 , \tag{2}$$

$$\frac{1}{\theta}\frac{d\theta}{dt} = \frac{1}{\rho c_p T}\frac{\partial}{\partial x_j}\left[\kappa\frac{\partial T}{\partial x_j}\right] , \tag{3}$$

with

$$\frac{d}{dt} = \frac{\partial}{\partial t} + u_i\frac{\partial}{\partial x_i} , \tag{4}$$

where g is the acceleration of gravity; $R = c_p - c_v$ and $\gamma = c_p/c_v$ the ratio of specific heats at constant pressure and volume, respectively; μ and κ the coefficients of viscosity and heat conduction; δ_{ij} is the Kronecker delta and the summation convention over repeated indices is assumed. We take x_1 in the direction of wave propagation, x_3 is the vertical coordinate with the ground at $x_3 = 0$; x_1, x_2 and x_3, form the usual right-handed triplet and u_1, u_2, and u_3 are the corresponding velocity components. The Coriolis force has been neglected.

We now decompose each variable $b(x_i,t)$ into the sum of a mean component $B(x_i)$, a periodic component $\tilde{b}(x_i,t)$, and a turbulent component $b'(x_i,t)$:

$$b(x_i,t) = B(x_i) + \tilde{b}(x_i,t) + b'(x_i,t) \quad . \tag{5}$$

The period τ of the periodic part of the disturbance is determined experimentally through spectral analysis of the time series of the pressure at the ground. When a large amplitude gravity wave is present, a large peak in the spectrum fixes τ unequivocally. The time independent part of the signal is obtained by applying the time average operator, denoted hereafter by an overbar:

$$B(x_i) = \bar{b}(x_i) = \lim_{T\to\infty} \frac{1}{T} \int_0^T b(x_i,t)dt \quad , \tag{6}$$

with T in practice chosen much larger than τ. To determine $\tilde{b}$ and b' we introduce the phase averaging operation < >

$$\langle b \rangle = B + \tilde{b} = \lim_{N\to\infty} \frac{1}{N} \sum_{n=1}^{N} b(t + n\tau) \quad , \tag{7}$$

which extracts the mean and wave component from the signal by averaging over a large ensemble of points having the same phase with respect to the gravity wave. The wave, therefore, acts as a reference oscillator (Hussain and Reynolds, 1972; Einaudi and Finnigan, 1981). It should be noted that the periodic component $\tilde{b}$ obtained by phase averaging will not, in general, be monochromatic and the harmonic content of the disturbance is fully retained by the phase averaging operation. The wavelike and the turbulent parts of the field variable b will then be given by

$$\tilde{b} = \langle b \rangle - B \quad , \tag{8}$$

$$b' = b - \langle b \rangle \quad . \tag{9}$$

If we now write

$$u_i = U_i + \tilde{u}_i + u_i'$$
$$\theta = \Theta + \tilde{\theta} + \theta'$$
$$p = P + \tilde{p} + p' \qquad (10)$$

and substitute (10) into (1)-(3) we can derive equations for the instantaneous values and moments of the wavelike and turbulent quantities. In what follows we denote the mean value of the temperature by T_0. The derivation is carried out in the Boussinesq approximation. Substitution of (10) into (1) and subtraction of its time average from its phase average gives the momentum equation for the periodic disturbance:

$$\frac{\partial \tilde{u}_i}{\partial t} + U_j\frac{\partial \tilde{u}_i}{\partial x_j} + \tilde{u}_j\frac{\partial U_i}{\partial x_j} = -\frac{1}{\rho}\frac{\partial \tilde{p}}{\partial x_i} + \nu\frac{\partial^2 \tilde{u}_i}{\partial x_j \partial x_j} - \frac{\partial \tilde{r}_{ij}}{\partial x_j} - \frac{\partial}{\partial x_j}(\tilde{u}_i\tilde{u}_j - \overline{\tilde{u}_i\tilde{u}_j}) + \frac{g}{\theta}\tilde{\theta}\delta_{i3}, \qquad (11)$$

with ν the kinematic viscosity and

$$\tilde{r}_{ij} = \langle u'_i u'_j \rangle - \overline{u'_j u'_j} \ . \qquad (12)$$

In the Boussinesq limit, time and phase averaging (2) gives

$$\frac{\partial U_i}{\partial x_i} = \frac{\partial \tilde{u}_i}{\partial x_i} = \frac{\partial u'_i}{\partial x_i} = 0 \ . \qquad (13)$$

Manipulation of (3) similar to that applied to (1) provides

$$\frac{\partial \tilde{\theta}}{\partial t} + U_j\frac{\partial \tilde{\theta}}{\partial x_j} + \tilde{u}_j\frac{\partial \Theta}{\partial x_j} = -\frac{\partial}{\partial x_j}\left[\tilde{u}_j\tilde{\theta} - \overline{\tilde{u}_j\tilde{\theta}}\right] - \frac{\partial}{\partial x_j}\tilde{r}_{j\theta} + \kappa\frac{\partial^2 \tilde{\theta}}{\partial x_j \partial x_j} \qquad (14)$$

where

$$\tilde{r}_{j\theta} = \langle u'_j\theta' \rangle - \overline{u'_j\theta'} \quad . \tag{15}$$

The $\tilde{r}_{ij}$ and $\tilde{r}_{j\theta}$ terms can be viewed as the wavelike fluctuations in the turbulent Reynolds stress and heat flux, respectively, due to the presence of the wave. Equations equivalent to (11) and (14) can be derived for the turbulent components.

Following Reynolds and Hussein (1972), Finnigan and Einaudi (1981), and Finnigan et al. (1984), we derive the conservation equations for the average kinetic energy density of wave and turbulent components, both for the average heat flux associated with the wave and for the variance of the wave temperature fluctuations:

$$\frac{d}{dt}\left[\overline{\frac{\tilde{u}_i\tilde{u}_i}{2}}\right] = -\frac{\partial}{\partial x_j}\left\{\overline{\tilde{u}_j\left[\tilde{p} + \frac{\tilde{u}_i\tilde{u}_i}{2}\right]}\right\} - \overline{\tilde{u}_i\tilde{u}_j}\frac{\partial U_i}{\partial x_j} + \tilde{r}_{ij}\overline{\frac{\partial \tilde{u}_i}{\partial x_j}}$$

$$- \frac{\partial}{\partial x_j}(\overline{\tilde{u}_i\tilde{r}_{ij}}) + \frac{g}{\bar{\theta}}\overline{\tilde{\theta}\tilde{u}_i}\delta_{i3} + \text{viscous terms} \quad , \tag{16}$$

$$\frac{d}{dt}\left[\overline{\frac{u'_iu'_i}{2}}\right] = -\frac{\partial}{\partial x_j}\left\{\overline{u'_j\left[p' + \frac{u'_iu'_i}{2}\right]}\right\} - \overline{u'_iu'_j}\frac{\partial U_i}{\partial x_j} - \tilde{r}_{ij}\overline{\frac{\partial \tilde{u}_i}{\partial x_j}}$$

$$- \overline{\tilde{u}_j\frac{\partial}{\partial x_j}\left[\frac{\tilde{r}_{ii}}{2}\right]} + \frac{g}{\bar{\theta}}\overline{u'_i\theta'}\delta_{i3} + \epsilon + \text{viscous transport} \tag{17}$$

$$\frac{d}{dt}\overline{\tilde{\theta}\tilde{u}_i} = -\overline{\tilde{u}_i\tilde{u}_j}\frac{\partial\Theta}{\partial x_i} - \overline{\tilde{\theta}\tilde{u}_j}\frac{\partial U_i}{\partial x_j} - \overline{\tilde{u}_i\frac{\partial}{\partial x_j}\tilde{r}_{j\theta}}$$

$$- \overline{\tilde{\theta}\frac{\partial}{\partial x_j}\tilde{r}_{ij}} - \frac{\partial}{\partial x_j}\overline{\tilde{\theta}\tilde{u}_i\tilde{u}_j} - \overline{\tilde{\theta}\frac{\partial\tilde{p}}{\partial x_i}} + \frac{g}{\bar{\theta}}\overline{\tilde{\theta}^2}\delta_{i3} + \text{viscous and conductive terms} \tag{18}$$

$$\frac{d}{dt}\overline{\tilde{\theta}^2} = -\overline{\tilde{\theta}\tilde{u}_j}\frac{\partial\Theta}{\partial x_j} - \frac{\partial}{\partial x_j}\overline{\tilde{u}_j\tilde{\theta}^2} - \overline{\tilde{\theta}\frac{\partial}{\partial x_j}\tilde{r}_{j\theta}} + \text{conductive terms.} \tag{19}$$

ϵ is the viscous dissipation of turbulent kinetic energy. In all the other equations the viscous and conductive effects are negligibl

Equations equivalent to (18) and (19) can be derived for the turbulent budgets.

Equations (11) through (14) will be discussed in the next section where the data will be compared with a linear solution. Equations (16) through (19) will be analyzed in Section 5.

4. The Linear Solution and its Limitations

In this section we present the data for two similar events which occurred on December 20, 1984, (event I) and on January 2, 1985 (event II). Event I will be discussed in detail while event II will be invoked only to provide corrobarating evidence for what we consider to be some of the most important conclusions concerning the behavior of event I. In this we make a virtue of necessity since during event II the fast response temperature sensors were not working and the budgets involving temperature information could not be completed.

The pressure traces for the eight microbarographs are plotted as a function of time in Fig. 2a for event I, and in Fig. 3a, for event II. Figure 2a covers a 60 min interval starting at 1040 MST while Fig. 3a aso starts at 1040 MST but continues for 100 min. All traces, while not as monochromatic as those described by Einaudi and Finnigan (1981), reveal a periodic behaviour confirmed by the power spectral plots of microbarograph 70 at the bottom of the tower. These are displayed in Fig. 2b and Fig. 3b. Time series of the three velocity components u_i for I are given in Figs. 4, 5, and 6, respectively, for each instrumented level. The temperature traces from the fast response sensors are plotted in Fig. 7. Figures equivalent to 4 through 7 are omitted for event II, but have the same general behavior. Time averages have been removed from each of the plots so that the signals in Figs. 2 through 7 are the sum of the periodic and the turbulent components only. The time series are completed by the

monostatic acoustic sounder records displayed in Fig. 8a and Fig. 8b for events I and II, respectively. The traces of the velocity components and of the temperature, although much noisier than those of the pressure, reveal the same periodic behavior, a fact confirmed by their spectra, not shown here. When a substantial gravity wave is present the pressure traces are invariably smoother than the velocity and temperature signals for two reasons. First of all the contribution of the wave pressure to the total signal, a contribution of larger scale and greater apparent smoothness than the turbulent pressure, exceeds the turbulent contribution, whose amplitude is of order $2.5\rho u_*^2$, u_* being the usual friction velocity, by at least an order of magnitude. Secondly, the contribution of velocity and temperature fluctuations over all space to the local pressure signal (a circumstance characterized by the Poisson equation for static pressure) biases the pressure signal towards lower frequencies.

The regularity of the records varies with height and the apparently nonlinear nature of some of the signals also varies with height. Particularly interesting in this regard is the highly nonlinear nature of the temperature trace at 100 m, a point to which we will return. The acoustic sounder records reveal height dependent reflections modulated by large oscillations. The reflections are proportional to the intensity of temperature fluctuations (Brown and Hall, 1978) which can be taken as some measure of the turbulence intensity.

We now determine the harmonic content of the wavelike disturbances and the speed with which they travel horizontally, that is, the horizontal phase speed. The spectral content is determined through an FFT routine spanning either a 2560 s or a 5120 s interval. Time series were tapered with a Hanning window to reduce side band leakage. Let τ be the dominant period, $f = 1/\tau$ and $\omega_r = 2\pi f$ be the circular and radian frequencies, respectively. The horizontal speed of propagation $\vec{v}_{ph}$ is determined in amplitude and direction by cross-correlating the pressure signals from all

eight microbarographs. No direct information is available on the horizontal scales λ of these disturbances since they are much larger than the size of the microbarograph network. The quantity λ is derived from the relation

$$\vec{v}_{ph} = \frac{\omega_r}{k} \frac{\vec{k}}{k} \tag{20}$$

where $k = 2\pi/\lambda$ is the amplitude of the wave number vector and ω_r/k is the amplitude of horizontal phase velocity.

The periods τ, horizontal phase speeds, wavelengths and peak to peak amplitudes of the disturbances for both events are summarized in Table 1. The values of these quantities and the nature of the data displayed in Figs.2 through 8 are consistent with those observed in other case studies carried out by the present authors, where an explanation of the observations was given in terms of an internal gravity wave generated by shear. Here too, therefore, we calculate the periods, horizontal wavelengths, and the corresponding vertical structure of all the thermodynamic variables for the range of internal gravity waves that the atmosphere can support and compare them with observations. Assuming that the amplitude of the disturbance is small compared with the mean fields, we linearize (10) and (13) and we use for the components U_1 and U_2 of the horizontal wind and the background temperature T_0, the smoothed values obtained from the rawinsonde launch from Denver airport that was closest to the time of the event. For event I, we used the launch at 2310 GMT December 20, 1984, which took place about 5 hours after the end of the event. This time difference together with the spatial separation (Denver is 25 miles south of the BAO) imply that our knowledge of the atmospheric state is approximate, a point to be kept in mind in judging the agreement between observations and model values.

The solution of the linearized equations of motion is then sought in the

form

$$\tilde{b}(x_1, x_3, t) = \hat{b}(x_3) \exp\left[i(\omega t - kx_1)\right] + \text{c.c.} \tag{21}$$

where c.c. stands for complex conjugate, $i = \sqrt{-1}$ and $\omega = \omega_r + i\omega_i$ will in general be complex. The x_1 axis has been chosen in the direction from west to east, which is the direction of the propagation of the disturbance in event I. For a horizontally homogeneous background state, which we assume here, the system can be described by the component of the background wind in the direction of wave propagation and by a solution which is independent of x_2. In fact, ω and k are the eigenvalues of a second order differential equation in x_3, the Taylor-Goldstein equation, to which the linearized system of original equations can be reduced by straightforward elimination of all variables but one. In terms of a variable $\hat{q}$ which is essentially the amplitude of the vertical displacement, the Taylor-Goldstein equation takes the particularly simple form

$$\frac{d}{dx_3}\left\{\frac{r\Omega^2}{\left[1 - \Omega^2/(k^2c^2)\right]} \frac{d}{dx_3}\hat{q}\right\} + k^2 r(n^2 - \Omega^2)\hat{q} = 0 \tag{22}$$

where

$$\Omega = \omega - k U_1 \tag{23}$$

$$n^2 = -g\left[\frac{1}{\rho_0}\frac{d\rho_0}{dx_3} + g/c^2\right] \tag{24}$$

$$r = \rho_0 \epsilon^2 \tag{25}$$

$$\epsilon = \exp\left[g \int_0^z \frac{dz'}{c^2(z')}\right] \tag{26}$$

$$q = \frac{Q_3(z)}{i\Omega\epsilon} \tag{27}$$

ρ_0 is the background density and c is the speed of sound. The quantity Ω is the Doppler-shifted frequency, n^2 is the square of the Brunt-Väisälä frequency, r is proportional to the background density and q is proportional to the vertical displacement.

To obtain equation (22) the Boussinesq approximation is not required. The latter was only used to derive the budget equations. The original problem is now reduced to determining the eigenvalues ω and k of (22) such that the corresponding eigenfunctions q satisfy the boundary conditions of zero vertical displacement at the earth's surface and the radiation condition at $z = +\infty$. The values of ω and k are determined by numerically integrating (22), following the approach of Lalas and Einaudi (1976). The background values of U_1 and T_0, discussed earlier and used to calculate the coefficients of (22) are plotted in Fig.9a,b. The Richardson number, R_i is defined by,

$$R_i = n^2/(dU_1/dx_3)^2 \tag{28}$$

In Figure 9c, Ri is given as a function of height. Of significance here is the fact that the values of the Richardson number derived from the raw data by linear interpolation have a minimum of about 0.38 in the 400-700 m range. Changes in background wind and, above all, in background temperature well within the experimental error of the rawinsondes can easily bring such values of R_i below 0.25. Experience indicates that such low values of R_i are a clear indication of region of dynamic instability in the atmosphere leading to unstable solutions of the kind given by (21). The analytical profile of R_i, obtained by mean square fitting U_1 and T_0 using hyperbolic tangent and Gaussian functions, reveals a dip below 0.25 in the 375-500 m range where the mean wind U_1 varies from 8 to 12.7 m/

The measured phase speed of 10.7 suggests that indeed the observed disturbance has a critical level there, where such a speed matches the mean wind, and where R_i has a minimum. Other minima in the R_i profile are not of interest here because they occur at levels where the mean winds and hence the phase velocity of any associated disturbances are much higher than the observed phase speed.

Having chosen $\tau = 427$ s and, therefore, having $\omega_r = 2\pi/\tau$ fixed, the values of ω_r/k and ω_i were determined numerically. The value of ω_i was $\omega_i = 4.9\ 10^{-4} s^{-1}$ corresponding to an e-folding time of 34 min. The remaining values are given in Table I. Aside from ω_i, which is small as in many other case studies, and for which we do not have experimentally determined values, the remaining eigenvalues τ and λ agree quite well with the measured ones. This suggests that, even though the individual signals at the various levels along the tower may display significant nonlinearities, the bulk parameters of the disturbance, such as period and horizontal wavelength, appear to remain those of the linear solution although this, in principle, is valid only for an infinitesimal amplitude. We will come back to this point later.

The comparison between observations and model results for the various variables is given in Figs. 10 and 11. In Fig. 10 the amplitudes of u_i, $i = 1,2,3$, and $\tilde{\theta}$ are plotted as functions of height. The data points are the amplitudes of the fundamental Fourier components of the phase averaged variables. The linear model solutions, which are only given within a constant multiple, have been scaled so that the model pressure at the ground matches the measured pressure at the base of the tower. As discussed earlier, the pressure is the measured variable least affected by local boundary-layer influences. Although the agreement for the vertical velocities is quite good, the agreement for the other variables is less satisfactory, at least at some levels. This disagreement can depend on a number of factors, the main one, we believe, being the substantial

differences in U_i and T_0 between Denver and the BAO due either to the geographical separation or the difference in time between the event and the rawinsonde launch. The difference in the micro climates of the two sites is likely to affect the measurements within the tower height more than higher up where the wave, if generated by shear, draws its energy. The agreement between the phases of data and model values in Fig. 11 is generally poor, except at a few levels. Similar considerations apply to case II.

The differences between data and model output for the amplitudes are well within the range observed in the three cases analyzed by Einaudi and Finnigan (1981) and Finnigan et al. (1984). The differences in the phases are much larger. We suggest two possible reasons for this. One is that indeed the differences in the background state between Denver and the BAO are larger in the present cases, especially for the background wind. the second reason is the neglect of nonlinear wave and turbulent terms in the equations. These terms will be discussed in the next section. Here it suffices to point out that such terms may influence the phase relations of the model output rather more than the amplitudes.

In discussing the wave budget, we will show that some success is obtained in closing the measured wave budget by using the model solution for the pressure with the measured $\tilde{u}_i$, a confirmation of the validity of the linear model.

All in all, we feel that the linear solutions provide, in general, a good estimate of the period and wavelength of the observed disturbances even though their amplitudes have reached some sort of steady state level, beyond the validity of linear theory. This is so probably because these quantities depend more on the wind and temperature structure near the critical level above the tower than on the structure lower down within the boundary layer. The actual amplitudes and phases for the thermodynamic variable , on the other hand, are much more critically dependent not only

on an accurate knowledge of the mean state, but also on nonlinear and turbulent terms.

5. Higher Moments of the Wave and Turbulence

Two kinds of "stress" divergence term appear in the momentum equations of individual wave components, $\tilde{u}_i$. Equation (11) illustrates this. The first of these, the non-linear wave shear stresses $\overline{\tilde{u}_1\tilde{u}_3}$ and $\overline{\tilde{u}_2\tilde{u}_3}$ are plotted in Fig. 12. Information about the magnitude of the normal components of $\overline{\tilde{u}_i\tilde{u}_j}$ $(i = j)$ is already contained in Fig. 10. We note that $\overline{\tilde{u}_1\tilde{u}_3}$ is significantly positive below 100 m implying *upward* momentum transport, while $\overline{\tilde{u}_2\tilde{u}_3}$ is slightly positive at 250 m.

This emphases that the behavior of the wave, a disturbance with vertical length scales of the same order or greater than the vertical scale over which the background wind varies, cannot be expected to behave as gradient diffusion theory conditions us to expect.

The second class of stress divergence terms is the $\tilde{r}_{ij}$'s, the wave period fluctuations in turbulent stresses. These terms are of crucial importance in coupling the wave and turbulence fields as we shall see in Section 6. In general, they play a significant role in the momentum budgets also. An order of magnitude comparison between $\tilde{u}_3\partial U_1/\partial x_3$ (taken as characteristic of the size of terms retained in the linear solution), $\partial\tilde{r}_{ij}/\partial x_j$ and $\partial\tilde{u}_i\tilde{u}_j/\partial x_j$ gives, when averaged over the tower height, $\left|\tilde{u}_3\frac{\partial U_1}{\partial x_3}\right| : \left|\partial\tilde{r}_{ij}/\partial x_j\right| : \left|\frac{\partial}{\partial x_j}\tilde{u}_i\tilde{u}_j\right| = 1:0.4:0.1$. Furthermore we have already alluded to the possibility that $\tilde{r}_{ij}$ terms in the momentum budgets affect the phases of the waves more than their amplitudes. Evidence for this viewpoint comes from the work of Hussein and Reynolds ( ), who modelled experimental measurements of wave disturbances in a turbulent channel flow in various ways. They were unable to reproduce the observed phase relationships between wave components without reproducing the *actual* phase

relationships between $\tilde{r}_{ij}$ and the velocity wave, although the velocity wave amplitudes could be recovered without reproducing the $\tilde{r}_{ij} - \tilde{u}_j$ phase relationship. Fua et al. ( ) have also commented on the large departures from linear model phase differences that can develop between wave components when $\tilde{r}_{ij}$ is modelled realistically. As we shall see in Section 6 the $\tilde{r}_{ij}$'s also play an essential role in inducing nonlinear behavior in the wave.

In Fig. 13a, we plot the height variation of $\tilde{r}_{11_0}$ $\tilde{r}_{22_0}$ and $\tilde{r}_{33_0}$ the fundamental Fourier components of $\tilde{r}_{11}$, $\tilde{r}_{22}$ and $\tilde{r}_{33}$ (all the plots of $\tilde{r}_{ij}$'s and $\tilde{r}_{j\theta}$'s will be of the amplitude of this fundamental component). Note the vanishingly small value of $\tilde{r}_{11_0}$ at 150 m and that $\tilde{r}_{33_0}$ is typically two orders of magnitude smaller than $\tilde{r}_{11_0}$. This does not mean, however, that either of these terms is insignificant, rather that they are composed almost entirely of higher harmonic contributions. The variation of the wave period fluctuations in turbulent shear stress, $\tilde{r}_{13_0}$ and $\tilde{r}_{23_0}$ appear in Fig.13b. In fact, all of these fundamental components except $\tilde{r}_{22_0}$ and $\tilde{r}_{33_0}$ have a minimum at ~ 150 m height. This we recall is where the temperature wave $\tilde{\theta}$ also displays clear nonlinearity (see Fig.7) and where the local stratification peaks.

Turbulent normal stresses $\overline{u'^2_1}$, $\overline{u'^2_2}$, and $\overline{u'^2_3}$ are displayed in Fig. 14a. Note the small near constant value of $\overline{u'^2_3}$, a feature not inconsistent with strong stratification, and the fact that $\overline{u'^2_2} > \overline{u'^2_1}$, which is also consistent with the differences in $\partial U_1/\partial x_3$ and $\partial U_2/\partial x_3$. Turbulent shear stresses plotted in Fig. 14b display no surprises.

Let us turn now to the heat fluxes; first the vertical wave heat flux $\overline{\tilde{u}_3\tilde{\theta}}$ shown in Fig. 15. The interesting point about this is that it is upwards, or counter-gradient between 75 m and 225 m. This important point will be treated at length in Section 6. The amplitude of the fundamental component of wave period variations in turbulent flux $\tilde{r}_{3\theta_c}$ is displayed in Fig. 16 and is almost an order of magnitude larger than the wave flux.

$\tilde{r}_{j\theta}$'s too play a central role in the energetics of the system. The turbulent heat flux depicted in Fig. 17 is countergradient over roughly the same height range and with the same magnitude as $\overline{\tilde{u}_3\tilde{\theta}}$. In this, it is distinctly different from the case discussed in Finnigan et al. (1984), where, although the wave heat flux was counter-gradient, the turbulent flux was cogradient, summing in the end to a small cogradient flux.

6. The Energetics of the Wave-Turbulence-Background System

In this section we discuss the kinetic energy budgets of the wave and turbulent velocities, the wave heat flux and the variance of the temperature fluctuations corresponding to eq's (3.16), (3.17), (3.18) and (3.19), respectively. Wherever possible, each discussion of Event I is followed by a comparison with the corresponding budgets for Event II and the other cases examined by the authors and mentioned above.

a. Wave kinetic energy budget

The budget of wave kinetic energy $\frac{1}{2}\overline{\tilde{u}_i\tilde{u}_i}$, although different in detail from others we have studied, displays features which we suggest are generic. We begin by displaying in Fig. 18 the various terms of equation (16) as functions of height. Gain terms are positive; they act to increase the wave kinetic energy in time, while loss terms are negative and act to decrease it. In the period under consideration, the wave amplitudes are essentially constant in time (see for example Fig. 2) so we expect the gain and loss terms to sum to zero at all heights.

The principal gain term is "shear production", $-\overline{\tilde{u}_i\tilde{u}_j}\frac{\partial U_i}{\partial x_j}$, the work done by the wave stresses against the mean rates of strain. The main contribution to this term comes from $-\overline{\tilde{u}_1\tilde{u}_3}\frac{\partial U_1}{\partial x_3}$ and $-\overline{\tilde{u}_2\tilde{u}_3}\frac{\partial U_2}{\partial x_3}$. We have no way of calculating the normal stress-horizontal gradient terms ($i = j$), but on general scaling ground we expect them to be much smaller than the shear terms.

The next largest gain term is buoyant production. In fact, this constitutes a gain between about 70 and 220 m and a loss outside this region. The presence of positive values of kinematic wave heat flux $\overline{\tilde{u}_3\tilde{\theta}}$ despite the strong stable stratification throughout the tower height (see Fig. 9c) obviously calls for explanation and we will return to consider this feature in detail below.

The third production term $\tilde{r}_{ij}\overline{\frac{\partial\tilde{u}_i}{\partial x_j}}$ represents a physical process playing a crucial role in the exchange of kinetic energy between the wave and turbulent fields. It describes the net work done by the wavelike fluctuations in turbulent stress, $\tilde{r}_{ij}$, against the fluctuating rates of strain, $\partial\tilde{u}_i/\partial x_j$. The same term appears with opposite sign in the equation (17) for turbulent kinetic energy so that it represents direct kinetic energy transfer between wave and turbulence. When either $\tilde{r}_{ij}$ or $\partial\tilde{u}_i/\partial x_j$ are dominated by their fundamental spectral component, then the mean product of any element of the term can be closely approximated by $\left|\tilde{r}_{\alpha\beta}\right|\cdot\left|\partial\tilde{u}_\alpha/\partial x_\beta\right|\cdot\cos\varphi$ (no sum over Greek indices), where φ is the phase angle between the two periodic signals. When $\varphi = (2n-1)\pi/2$, then the net work done is zero. In a nearly neutrally stratified boundary layer, Finnigan and Einaudi (1981) observed this phase angle to be close to $\pi/2$, the quadrature relationship predicted by rapid distortion theory in the limit of very long waves (Hunt and Maxey, 1978). A quadrature relationship of this kind permits the coexistence of large amplitude $\tilde{r}_{ij}$'s and wave strains with no net energy transfer. In a stably stratified boundary layer, in contrast, Finnigan et al. (1984) observed the phase angle φ to move to about $\pi/4$ with a consequent transfer of kinetic energy from wave to turbulence.

A more extensive survey of the dependence of φ on stratification was published by Finnigan (1988) who compared nine different events with stratification varying between near neutral and strongly stable. He found that, if a significant temperature wave were present, a circumstance

requiring, but not automatically following from stable stratification, the quadrature relationship of neutral stability disappeared and the wave lost kinetic energy to the turbulence.

The principal components of $\overline{\tilde{r}_{ij}\partial\tilde{u}_i/\partial x_j}$ are $\overline{\tilde{r}_{13}\partial\tilde{u}_1/\partial x_3}$ and $\overline{\tilde{r}_{23}\partial\tilde{u}_2/\partial x_3}$ and in the present case, the second of these makes the dominant contribution. If we write the Fundamental Fourier components of $\tilde{r}_{ij}$ and $\partial\tilde{u}_i/\partial x_j$ as $\tilde{r}_{ij_0}$ and $(\partial\tilde{u}_i/\partial x_j)_0$ then φ_{13} and φ_{23}, are the phase angle differences between $\tilde{r}_{13_0}$ and $(\partial\tilde{u}_1/\partial x_3)_0$ and $\tilde{r}_{23_0}$ and $(\partial\tilde{u}_2/\partial x_3)_0$, respectively. These angles are plotted against x_3 in Fig. 19. In the height range 75-275 m, φ_{23} was $-\pi/3$, implying transfer of energy from wave to turbulence and overriding the contribution from $\overline{\tilde{r}_{13}\partial\tilde{u}_1/\partial x_3}$ which had $\varphi_{13} \sim 3\pi/4$ below 200 m, implying that this term was transferring energy from turbulence to wave. Below 75 m, both components indicate transfer of energy from turbulence to wave as the profile of the total term (Fig. 19), which includes contributions from all Fourier components, confirms. Above ~ 200 m both phase angles indicate a transfer of energy from wave to turbulence. One note of caution should be sounded; when the $\tilde{r}_{ij}$'s have significant higher harmonic content, which is particularly true near the ground, the quadrant of φ may give a misleading indication of the sign of the total interaction.

We have estimated the magnitude of the normal contributions $\overline{\tilde{r}_{\alpha\alpha}\partial\tilde{u}_\alpha/\partial x_\alpha}$, $\alpha = 1$, $\alpha = 2$ using the hypothesis: $\partial\tilde{u}_1/\partial x = ik\tilde{u}_1$, and $\partial\tilde{u}_2/\partial x_2 = ik\tilde{u}_2$. Although $|\tilde{r}_{11}|$ and $|\tilde{r}_{22}|$ are comparable to $|\tilde{r}_{13}|$ and $|\tilde{r}_{23}|$, $ik\tilde{u}_1$ and $ik\tilde{u}_2$ are an order of magnitude smaller than the fluctuating vertical gradients because of the long wavelength (~ 4 km) of the wave. $\overline{\tilde{r}_{33}\,\partial\tilde{u}_3/\partial x_3}$ could be calculated directly and was negligible.

The transport terms, $-\partial/\partial x_j\overline{\tilde{u}_i\tilde{u}_i\tilde{u}_j}$ and $-\partial/\partial x_j\overline{\tilde{u}_i\tilde{r}_{ij}}$ are small except below 75 m where the second of these is the major loss term. This close to the ground the turbulence is generally stronger than at higher levels. There is also much more harmonic content in the phase averaged velocity wave forms, (Figs. 4, 5, and 6), and in the $\tilde{r}_{ij}$'s, (Fig. 13). Indeed, in the

near-ground region the oscillations (with x_3) of most of the terms in the budget suggest the possible existence of transient growing or decaying modes coupled to the ground based "viscosity wave", the extra eigenfunction that must be added to the inviscid solution to satisfy a boundary condition of no slip at the ground (Jones and Hooke,).

The imbalance in the budget is plotted as the "loss" term that satisfies the equation. Into this term are consigned all of the quantities we are unable to measure but estimate to be small, such as horizontal advection, the time derivative, and terms involving instantaneous horizontal gradients. However, we expect the largest contribution to the imbalance term to come from the "pressure transport" $-\frac{\partial}{\partial x_3}\overline{\tilde{p}\tilde{u}_3}$, the divergence of the classical wave energy flux. Unlike the analogous term in the turbulent budget, the pressure term in the wave budget cannot be regarded as a transport term in the sense of rearranging energy within the boundary layer. Rather, it provides a connection with the source of wave energy at the critical level; within the compass of linear theory, $\overline{\tilde{p}\tilde{u}_3}$ is the only component of the flux of wave energy in the vertical.

Finnigan and Einaudi (1981) and Finnigan et al. (1984) had some success in closing the wave budget with the help of the linear model solution. The method used was to combine the linear model solution for $\tilde{p}(x_3,t)$ with measured $\tilde{u}_3(x_3,t)$ to obtain the desired term. This worked surprisingly well in neutral stratification (Finnigan and Einaudi 1981), but not particularly well in the strongly stable case (Finnigan et al. 1984). The result of the same procedure is compared with the imbalance term in Fig. 20. The quality of the agreement falls somewhere between the two earlier studies. The vertical variation of the term is reproduced rather well, but the agreement in absolute magnitude is not good. Nevertheless, Fig. 20 does offer independent and encouraging confirmation of the validity of both the linear model calculation and the computed budget.

The essential distinguishing features of this event as characterized by

the kinetic energy may be noted. The wave field extracts energy from the background wind and temperature fields within the boundary layer via shear and buoyant production. Some of this wave energy is converted to turbulent kinetic energy through the interaction term, $\overline{\tilde{r}_{ij}\partial\tilde{u}_i/\partial x_j}$. The rest is available to be transported out of the boundary layer by wave pressure transport $-\frac{\partial}{\partial x_3}\overline{\tilde{p}\tilde{u}_3}$. This state of affairs is not what we expect from classical linear wave theory, where the budget would have been a balance between pressure transport, a gain, and buoyant production, a loss. It is, however, consonant in its essential features with the other, essentially nonlinear ones that we shall now review.

We turn first to the budget of wave kinetic energy for the second new case presented here, Event II. The distribution of all the terms with height is different from the case we have just discussed, but it has two essential points of qualitative similarity, see Fig. 21. Firstly, over the middle range of heights, the coupling term $\overline{\tilde{r}_{ij}\partial\tilde{u}_i/\partial x_j}$ represents a loss of wave energy to turbulence, although it changes sign at higher levels and near the ground. Secondly, and more significantly, buoyant production is a gain, denoting, in this stably stratified case, countergradient heat flux.

We turn next to the first of the two events described in Finnigan et al. (1984). Once again, although differing in detail, the general features of the budget are similar. The wave-turbulence interaction term $\overline{\tilde{r}_{ij}\partial\tilde{u}_i/\partial x_j}$ comprised a loss of wave energy at most heights. Buoyant production was the dominant gain term, implying a strongly countergradient wave heat flux. Other terms such as transport, $-\frac{\partial}{\partial x_j}\left[\overline{\tilde{u}_i\tilde{u}_i\tilde{u}_j} + \overline{\tilde{u}_i\tilde{r}_{ij}}\right]$ were a loss at most heights as was shear production below 175 m. Like the present case, the wave *gained* energy from the mean field in the boundary layer and exported it to higher levels via the pressure term, $-\frac{\partial}{\partial x_j}\overline{\tilde{p}\tilde{u}_j}$, the presumed main component of the budget imbalance.

The budget described by Finnigan and Einaudi (1981) in a boundary layer only slightly stably stratified, while differing again in detail, displays

a loss of energy to turbulence and a gain through buoyant production implying, once more, countergradient heat flux. The main difference between this near neutral case and the more stable cases we have presented is that above 100 m the wave loses energy to both the mean field through shear production and to the turbulence, requiring a net supply of energy from above through the pressure transport term, $-\frac{\partial}{\partial x_j}\overline{\tilde{p}\tilde{u}_j}$.

A distinctive feature of all these budgets is a countergradient heat flux. In the more stable cases, this provides the dominant production term. Countergradient heat fluxes have been identified in many other stable events where waves are present, but budgets are not presented. See, for example, Finnigan (1988), Li et al. (1983), and Hunt et al. (1983). This means that when stratification is strong, the wave obtains energy from the background temperature field, within the boundary layer, although this behavior contracts to the lowest levels in our one near-neutral case (Finnigan and Einaudi 1981).

b. Wave heat flux

These considerations lead naturally to an investigation of the wave heat flux budget, equation (18). The question we pose is "how is an upwards heat flux maintained despite a positive temperature gradient in the essentially one-dimensional, stationary circumstances of the present cases and that studied by Finnigan and Einaudi (1981) and in the one-dimensional but nonstationary events discussed by Finnigan et al. (1984)"?

The wave heat flux budget for event I is plotted in Fig. 22. It is essentially a simple balance between a gain through buoyant production, $\frac{g}{T_0}\overline{\tilde{\theta}^2}$ and a loss to pressure destruction (as it is usually termed), $-\overline{\tilde{\theta}\partial\tilde{p}}/\partial x_3$. This we assume is the main component of the imbalance term. We have not had any success in matching the residual imbalance using the pressure gradient obtained from the linear model. This is in contrast to

the case of the energy budget, the essential point of difference being that, while the amplitude of the model derived pressure is roughly correct, its gradient is substantially smaller than what is required to close the heat flux budget. At this juncture, it is worth making a further point about the nature of the wave heat flux. The contribution of the oscillations in $\tilde{u}_3$ and $\tilde{\theta}$ at the fundamental frequency to the total flux $\overline{\tilde{\theta}\tilde{u}_3}$ can be written as $\overline{\tilde{\theta}_0\tilde{u}_{3_0}} = \left|\tilde{\theta}_0\right|\left|\tilde{u}_{3_0}\right| \cos\varphi$, where subscript o denotes here too the fundamental Fourier component and φ is the difference in phase angle. The phase of $\tilde{\theta}_0$ and $\tilde{u}_{3_0}$ relative to the pressure at the base of the tower is shown in Fig. 11b. Over most of the height range, φ takes on a value which makes $\overline{\tilde{\theta}_0\tilde{u}_3}$ opposite in sign to the total measured $\overline{\tilde{\theta}\tilde{u}_3}$, which is plotted in Fig. 15. Hence, $\overline{\tilde{\theta}_0\tilde{u}_{3_0}} \cos\varphi$ is co-gradient and the dominant contribution to $\overline{\tilde{\theta}\tilde{u}_3}$ must come from non-linear interaction between the wave velocity and temperature fields. We should not be surprised at this as we have already identified the domaint term maintaining heat flux as $\frac{g}{T_0}\overline{\tilde{\theta}^2}$.

The lack of significant transport terms in the heat flux budget, as is clearly apparent in Fig. 22, simply rephrases our original question to one of "how is a large amplitude temperature wave maintained in the stable boundary layer where the local Richardson Number has a large positive value"?

c. Variance of wave temperature

We turn, therefore, to the $\overline{\tilde{\theta}^2}$ budget, equation (19), which is plotted in Fig. 23. Here we see that the most significant loss term is $-\overline{\tilde{u}\tilde{\theta}}\partial T_0/\partial x_3$. If we define the wave potential energy as $\frac{1}{2}g/T_0\left[\frac{\partial\theta}{\partial x_3}\right]^{-1}\overline{\tilde{\theta}^2}$, which we may think of as the potential energy stored in parcels of fluid displaced from their mean position in the temperature gradient $\partial\theta/\partial x_3$ by wave motion (Finnigan et al. 1984), then we may interpret the term

$-\overline{\tilde{u}_3\tilde{\theta}}\partial\Theta/\partial x$ as a loss of wave potential energy to the mean potential energy field.

The two principal gain terms both represent non-linear processes. The first is the divergence of the triple moment, $\frac{\partial}{\partial x_j}\overline{\tilde{u}_j\tilde{\theta}^2}$, while the other involves the turbulence; it is the product of the temperature wave and the gradient of wavelike fluctuations in turbulent heat flux, $\overline{\tilde{\theta}\frac{\partial}{\partial x_j}\tilde{r}_{j\theta}}$. The time evolution $\frac{\overline{\partial\tilde{\theta}^2}}{\partial t}$ is difficult to assess, but amounts in total to a small loss while the residual imbalance is at least smaller than any of the directly measured components. In this, the only budget that contains no pressure terms and where the residual is a combination of measurement error and those terms containing unmeasurable horizontal gradients, the relatively small imbalance is reassuring.

The crucial point to be stressed is that the maintenance of the temperature wave, and in turn the countergradient heat flux and wave kinetic energy in the face of strong stable stratification, is the result of wave nonlinearity in which the presence of turbulence plays an essential role.

Practically the same story can be read in the wave heat flux, and the temperature variance budgets reported in the strongly nonstationary case of Finnigan et al. (1984). Although on that occasion, gradient production, $-\overline{\tilde{u}_i\tilde{u}_j}\frac{\partial\Theta}{\partial x_j}$ played a greater role in the heat flux budget, the $\overline{\tilde{\theta}^2}$ budget was practically identical and about the same quality of closure was obtained. The second case presented for the first time in this paper, Event II, had similar features, although we have not presented the budgets since the absence of fast temperature data made it impossible to calculate the crucial turbulence interaction term.

d. Turbulent kinetic energy budget

Before attempting to summarize the dynamics, let us turn to the turbulent

kinetic energy budget, Equation (17). This is presented in Fig. 24. The largest gain term is shear production, $-\overline{u'_i u'_j}\frac{\partial U_i}{\partial x_j}$ and the same problems occur here as in the wave budget when we come to consider mean horizontal gradients. The case of instantaneous horizontal gradients is more difficult than for the wave budget since we cannot make the convenient assumption that turbulent fluctuations behave like propagating waves.

The next most important gain term is buoyant production, at least over mid-tower height, denoting, as for the wave, countergradient flux. In this the present budget differs from the strongly stable case of Finnigan et al. (1984), where turbulent heat flux was towards the ground, although the wave flux was positive. In the near neutral case of Finnigan and Einaudi (1981) turbulent buoyant production was negligible.

The largest explicitly calculated loss term is viscous dissipation. This was calculated from the frequency spectra of u'_3 using normal inertial sublayer formula and assuming a Kolmogorov constant of 0.5.

The salient features of the stably stratified turbulence budgets, both the present case I, case II, which we have not presented, and those discussed by Finnigan and Einaudi (1986), bear similarities to the corresponding wave budgets in that, although there is significant direct transfer of kinetic energy from wave to turbulence via the coupling term $-\overline{\tilde{r}_{ij}\frac{\partial \hat{u}_i}{\partial x_j}}$, most of the turbulence gain relies on interactions with the mean field either through shear production or, in the latest case, shear *and* buoyant production.

7. Discussion and Conclusions

Let us, therefore, attempt to summarize the wave-turbulence energetics and clarify the questions that it raises about the behavior of the system as a whole. First of all, and most important in terms of the *essential* role of the wave, is the value of the gradient Richardson Number, Ri, within

tower height. In the stably stratified cases, it is very large at all levels, rarely dropping below 5. With Richardson numbers in this range, we do not expect to observe turbulence except possibly remnant "fossil" turbulence generated earlier and elsewhere that has evolved to a quasi permanent, two-dimensional structure. This kind of turbulence, while possibly relevant in some larger scale geophysical and oceanographic contexts, is not what we observe in the boundary layer. On the other hand we do observe continuous turbulence in the presence of internal gravity waves generated above the boundary layer. Large positive Richardson numbers deny the possibility of steady, local generation of the turbulence and we must seek for explanations in the unsteadiness and non-locality engendered by the wave.

The problem falls naturally into parts: We ask firstly, "can the arrival of a wave conjure turbulence from an initially laminar boundary-layer?" and secondly, "what are the mechanisms that govern the steady state, which may eventually emerge?" The first of these questions has been addressed by Jones and Hooke ( ). They pointed out that the viscosity wave that linear theory requires to be added to the inviscid eigensolutions of the system in order to satisfy a no-slip condition at the surface, is attenuated in the vertical over a distance that scales with the viscosity. If only molecular viscosity is availabe to transfer shearing stress, the wave attenuates in a few tens of centimeters, but if a realistic eddy viscosity is admitted, the depth of influence of the viscosity wave increases by one or two orders of matnigude. Furthermore, Jones and Hooke showed that the presence of an initial viscosity wave with a small eddy viscosity caused by a thin layer of weak turbulence near the ground, would lead within a few wave cycles to rapid growth of both wave and turbulence, at least as parameterized by eddy viscosity. All that is initially required in their paradigm is weak turbulence near the surface.

We know that in quasi steady state, a real viscosity always constitutes a

sink for kinetic energy, but when waves are present, the viscosity should be treated as a complex quantity with a definite, nonzero phase relationship between $\tilde{r}_{ij}$ and $\frac{\partial \tilde{u}_j}{\partial x_j}$. We have already pointed out that this phase relationship is $\sim \pi/2$ in neutral stratification and takes a range of values in stable times. Fua et al. (1982) took account of this implicit relaxation in the eddy viscosity in their one-and-a-half order closure model of wave turbulence interaction. They showed that in the initial growth stages of the wave, the relative phases of $\tilde{r}_{ij}$ and $\partial \tilde{u}_i/\partial x_j$ were such as to facilitate energy transfer from the background to the wave via the turbulence. This led in some cases to explosive wave growth.

The assumptions implicit in both these treatments of wave-turbulence interaction are that the turbulence is of small scale relative to the vertical wave gradients (use of an eddy viscosity) and that the turbulence adjusts rapidly to the changing background state (use of a time varying Richards Number to characterize turbulence production). Neither of these assumptions can be sustained in the steady state condition to which the system evolves and indeed may not be truly valid at any stage of the turbulence growth.

For example, in the case studied by Finnigan et al. (1984) the peaks in turbulence power spectra for each component at each height correspond to periods of around 300 s, which is similar to the wave period of 320 s. A similar situation obtains in the present case with a wave period of 427 s and spectral peaks around 350 s.

In the steady state case to which the system eventually evolves, the presence of the wave effectively destabilizes the system so that both wave and turbulence can gain energy from the background wind and temperature fields in the boundary layer. Hence, the present authors must abandon their earlier, somewhat naive view that the flow of kinetic energy was from the background state at the critical level into the wave, and thence by pressure transport, $-\frac{\partial}{\partial x_3}\overline{\tilde{p}\tilde{u}_3}$, into the boundary layer where the wave lost

energy to the turbulence and the background wind and temperature fields. The turbulence in turn would lose energy to dissipation, but was maintained by the flow of energy from the wave (Finnigan and Einaudi 1981). This picture, which was a reasonable description of the near neutral case they presented then, is obviously not in agreement with the more extensive body of data on stable boundary layers we now have and in the following paragraphs we shall attempt to replace it with a different, heuristic model. Much of what we shall say is based upon the detailed examination of the evolution of velocity component variance budgets through a wave cycle, which is contained in Finnigan et al. (1984).

In all of the cases we have studied, including the present one, the component $\overline{\tilde{r}_{33}\partial\tilde{u}_3}/\partial x_3$, that represents the direct flow of wave kinetic energy into $\overline{u'^2_3}$, is negligible. This means that almost all of the wave energy lost to turbulence through the $\overline{\tilde{r}_{ij}\partial\tilde{u}_i/\partial x_j}$ interaction term goes into horizontal turbulence fluctuations, $\overline{u'^2_1}$ and $\overline{u'^2_2}$. This horizontal turbulent kinetic energy (tke) is then transformed to $\overline{u'^2_3}$ by pressure-strain interaction, $-\overline{p'\partial u'_i}/\partial x_j$. In steady state, simple shear flows this energy conversion process is continuous, but in the presence of a wave causing periodic changes in stratification, significant transfer of energy to $\overline{u'^2_3}$ only occurs when the stratification is at a minimum. We can explain this by noting that pressure-strain transfer is an essentially three-dimensional interaction. In a stratified fluid we can place an upper limit, L_w, on the scale of vertical motion defined as $L_w(t) = \langle\overline{u'^2_3}\rangle^{\frac{1}{2}}/\langle n\rangle$, $\langle n\rangle$ being the phase average of the instantaneous Brunt-Väisälä frequency (Finnigan et al. 1984). The smaller $\langle n\rangle$ is, the greater the range of eddies that can be three-dimensional and acquire vertical kinetic energy at the expense of horizontal.

Altough we have not calculated the pressure-strain term directly, theoretical support for this picture is provided by the rapid- istortion calculations of a strati ed shea flow by Hunt et al. (and th

direct numerical simulations of Riley and Metcalf ( ), while experimental support can be found in Finnigan et al. (1984).

The vertical flux of heat, which is caused locally by turbulent mixing across the local temperature gradient, therefore, oscillates through a wave cycle, reaching a maximum when $n^2(t)$ is a minimum and $\langle u_3^2 \rangle$ at a maximum. In other words, the redistribution or smoothing out of the local temperature gradient is maximal at a particular phase of the wave.

This has immediate consequences of interest to our argument: firstly, an initial distribution of sinusoidal temperature waves rapidly acquires higher harmonic or "nonlinear" content; secondly, $\tilde{r}_{3\theta}$, the leading component of $\tilde{r}_{j\theta}$ the wave period fluctuation in turbulent heat flux, is well correlated with the distorted $\tilde{\theta}$. Thirdly, the onset of nonlinearity in $\tilde{\theta}$ produces attendant nonlinearity in $\tilde{u}_3$ because of the presence of the buoyant acceleration term $g\tilde{\theta}/T_0$ in the vertical component of the momentum equation (11).

The end result is to produce significant nonlinear interaction between $\tilde{u}_3$ and $\tilde{\theta}$ with the consequences we have already noted, particularly the countergradient heat flux and positive buoyant production of wave and turbulence kinetic energy. The essential role of the coupling between oscillating turbulent heat flux and nonlinear temperature wave can be seen in the vital contribution that the term directly representing this, $\overline{\tilde{\theta}\frac{\partial}{\partial x_j}\tilde{r}_{j\theta}}$, makes both in the $\overline{\tilde{\theta}^2}$ budget of the present case and in the nonstationary case of Finnigan et al. (1984). The initial production of horizontal tke from the shear is equally important since without this there is no vertical turbulence, hence our interest in the phase relationships of the elements of the $\tilde{r}_{ij}\frac{\partial \tilde{u}_i}{\partial x_j}$ terms considered as a whole.

The energetics we have described rely on two essential ingredients, both provided by the gravity wave:

1. Nonstationarity - This allows the production of $\overline{u'^2_1}$ and $\overline{u'^2_2}$ to decouple from ' and allows nonlinearity to grow in ' because of preferred vertical

mixing of temperature at one phase of the wave.

2. Nonlocality - The final $\tilde{u}_3$ and $\tilde{\theta}$ wave forms are a combination of the linear solution, a function of the state of the whole boundary layer and the troposphere above, and the local modifying effects of turbulence.

The data we have presented in this and previous paper differ substantially from what is observed in stable boundary layers when waves are not present, but the boundary layer is stationary and horizontally homogeneous. One of the best documented set of such data is that published by Nieuwstadt (1984). In order to allow continuous generation of turbulence, the gradient Richardson number must be less than 0.25 according to the classical inviscid treatment of Miles and Howard (1961) although various theoretical turbulence closure models reviewed by Nieuwstadt suggest $Ri \leq 0.22$ as a limiting value. Nieuwstadt's data also lack the extreme variability with height that is often observed in high Richardson number, wave perturbed cases. See for example the acoustic sounder facsimiles reported by Gossard et al. (1984), the data of Li et al. ( ) and the cases by the present authors discussed above.

In these cases, the spacing of the layers of strong acoustic return or the vertical "periodicity" of turbulence moments and budgets is usually similar to the vertical wavelength of the "eddy viscosity wave" that is needed to satisfy the no-slip condition at the surface, Jones and Hooke ( ). Of course we know that such a model is vastly oversimplified, but its length scale, a few tens of meters, is indicative of the scale of vertical variability we may expect.

An important consequence of this difference is that, while Nieuwstadt was able to propose and verify local similarity scaling for his stable turbulent layer based upon a local analogue of the Monin-Obukhov length, the prospects for finding an equivalent scaling for wave driven turbulence are more remote. The minimum that would be required is knowledge of a few critical wave parameters as well as the kind of local information used

Nieuwstadt's scheme. These wave parameters might include the height of the critical level, the amplitude of wave and temperature fluctuations there and the wave period. The horizontal wavelength of the disturbance is probably less important because it is usually so much larger than the depth of the boundary layer that the wave may be considered as providing a periodic shear and n^2. Of more value, but not usually available, would be the vertical wavelength of the eddy viscosity wave. We hope to consider these points at appropriate length in another publication.

Acknowledgements

The authors would like to thank Dr W. Neff for providing the microbarograph facsimile records and Dr J.C. Kaimal for his invaluable help and encouragement throughout this work. This research was supported by NSF Grant ATM-8213784.

TABLE 1

	Event I 1040-1140 MST 20 Dec. 1984		Event II 1040-1140 MST 2 Jan. 1985	
	Measured	Calculated	Measured	Calculated
Period τ (s)	427 $\pm$ 10	427 (assumed)	427 $\pm$ 10	427 (assumed)
Growth rate ω_i (s^{-1})	-	$4.9\ 10^{-4}$	-	$4.2\ 10^{-4}$
Phase speed (m/s)	10.7	9.5	7	5.7
Azimuth (degrees from North)	270	270 (assumed)	330	330 (assumed)
Horizontal wavelength (km)	4.6	4.1	3	4.6
Peak to Peak (μb)	88	88 (assumed)	180	180 (assumed)

Figure Captions

1. (a) Location map for the BAO

   (b) Microbarograph deployment at the BAO.

2. (a) Time series of pressure from the eight microbarographs for the period 10.40 – 11.40 MST on December 20, 1984 (Event I). The identification number of the microbarograph (refer to Fig. 1) is given at the left.

   (b) Spectrum of microbarograph 70 plotted in area preserving form. The vertical scale is arbitrary. The spectral peak corresponding to the wave we are studying is identified by an arrow. Note that these spectra have not been corrected for the high pass filter built into the microbarograph so the relative magnitude of the spectral peaks is misleading; most of the variance is associated with the marked peak of 427 s period.

3. (a) As in Fig. 2a but for event II (Jan 2, 1985). Note the longer record length.

   (b) As in Fig. 2b but for event II.

4. Time series of $(\bar{u}_1 + u'_1)$ from each level of the tower during event I. The traces are identified by instrument height in metres on the left.

5. As in Fig. 4 but for $(\bar{u}_2 + u'_2)$.

6. As in Fig. 4 but for $(\bar{u}_3 + u'_3)$.

7. As in Fig. 4 but for $(\tilde{\theta} + \theta')$.

8. (a) Monostatic Acoustic sounder facsimile record for Event I.

   (b) As in Fig. 8a but for event II.

9. (a) Measured and fitted profiles of background wind vs (x_3); Main figure: Rawinsonde data .; fitted profile used for stability analysis ————. Inset: subscript $_t$ refers to values measured on BAO tower. Fitted profile —•——•—.

   (b) As in (a) but for background temperature T_0.

   (c) As in (a) but for Richardson Number.

10. Comparison of linear solution and the amplitude of the fundamental Fourier component of the phase averaged data. , linear solution; —— , data.

11. Comparison of the linear solution and the phase of the fundamental Fourier component of the phase averaged data. The phase angles are plotted relative to the pressure at the ground, i.e. $\lfloor\tilde{p}$ is 0^o.

   (a) □ , $\lfloor\tilde{u}_1$ analytic solution; ▲, $\lfloor\tilde{u}_2$ analytic solution; —— $\lfloor\tilde{u}_1$ measurement; --- , $\lfloor\tilde{u}_2$ measurement.

   (b) ▲$\lfloor\tilde{u}_3$ analytic solution; □ , $\lfloor\tilde{\theta}$ analytic solution; —— $\lfloor\tilde{u}_3$ measurement; --- $\lfloor\tilde{\theta}$ measurement.

14. ertical profiles of measured eye sha

13. (a) Vertical profiles of the amplitudes of the fundamental Fourier components of $\tilde{r}_{11}$, $\tilde{r}_{22}$ and $\tilde{r}_{33}$.

(b) As for 13a but for $\tilde{r}_{13}$ and $\tilde{r}_{23}$.

14. (a) Vertical profiles of turbulent normal stress.

(b) Vertical profiles of turbulent shear stress.

15. Vertical profile of wave heat flux.

16. Vertical profile of the amplitude of the fundamental Fourier component of $\tilde{r}_{3\theta}$.

17. Vertical profile of the turbulent heat flux.

18. The terms of the wave kinetic energy budget for I (Equ. 16) plotted as a function of height. Gain terms are positive, loss terms negative.

——, $\overline{-\tilde{u}_i\tilde{u}_j}\,\frac{\partial U_j}{\partial x_j}$; – – –, $\overline{\tilde{r}_{ij}\,\frac{\partial \tilde{u}_i}{\partial x_j}}$; —.—. $\frac{g}{T_0}\,\overline{\tilde{u}_3\tilde{\theta}}$;

— — —, $-\frac{\partial}{\partial x_j}\,\overline{\tilde{u}_i\tilde{u}_i\tilde{u}_j}$; ----, $-\frac{\partial}{\partial x_j}\,\overline{\tilde{u}_i\tilde{r}_{ij}}$; — — —, residual

19. (a) Polar plot of φ_{13}, the phase difference between $\tilde{r}_{13_0}$ and $(\partial\tilde{u}_1/\partial x_3)_0$. Data points represent averages over the first 40 mins and second 40 mins of the 1 hour period. The plotted line is the average of these values.

(b) As in (a) but for φ_{23}.

20. Comparison of the residual term in the wave energy budget (Fig. 18) and the pressure transport term $-\frac{\partial}{\partial x_3}\overline{\tilde{p}\tilde{u}_3}$ computed by combining $\tilde{p}$ from the linear solution with measured $\tilde{u}_3$.

21. Wave kinetic energy budget for event II; legend as in Fig. 18. The residual is not plotted.

22. Wave heat flux budget (equation 18).

——, $-\overline{\tilde{u}_3^2}\frac{\partial \Theta}{\partial x_3}$; — — —, $-\overline{\tilde{\theta}\frac{\partial}{\partial x_j}\tau_{3j}}$; - - - - , $-\overline{\tilde{u}_3\frac{\partial}{\partial x_j}\tau_{j\theta}}$

— — —, $\frac{g}{T_0}\overline{\tilde{\theta}^2}$; ——, residual; — — —, $-\overline{\tilde{\theta}\frac{\partial \tilde{p}}{\partial x_3}}$ (calculated using linear model $\tilde{p}$ and measured $\tilde{\theta}$.)

23. The budget of wave temperature variance $\overline{\tilde{\theta}^2}$ (equ. 19).

——, $-\overline{\tilde{u}_3\tilde{\theta}}\frac{\partial \Theta}{\partial x_3}$; — — —, $\overline{\tilde{\theta}\frac{\partial}{\partial x_3}\tau_{3\theta}}$; —.—., $-\frac{\partial}{\partial x_3}\overline{\tilde{u}_3\tilde{\theta}^2}$;

——, residual.

24. The turbulent kinetic energy budget (eqn. 17) for case I.

——, $-\overline{u_i'u_j'}\frac{\partial U_i}{\partial x_j}$; ----, $-\overline{\tau_{ij}\frac{\partial \tilde{u}_i}{\partial x_j}}$; —.— $\frac{g}{T_0}\overline{\theta' u_3'}$

-----, $-\frac{\partial}{\partial x_j}\overline{u_i'u_i'u_j'}$; — — — , viscous dissipation ;

— — — , residual.

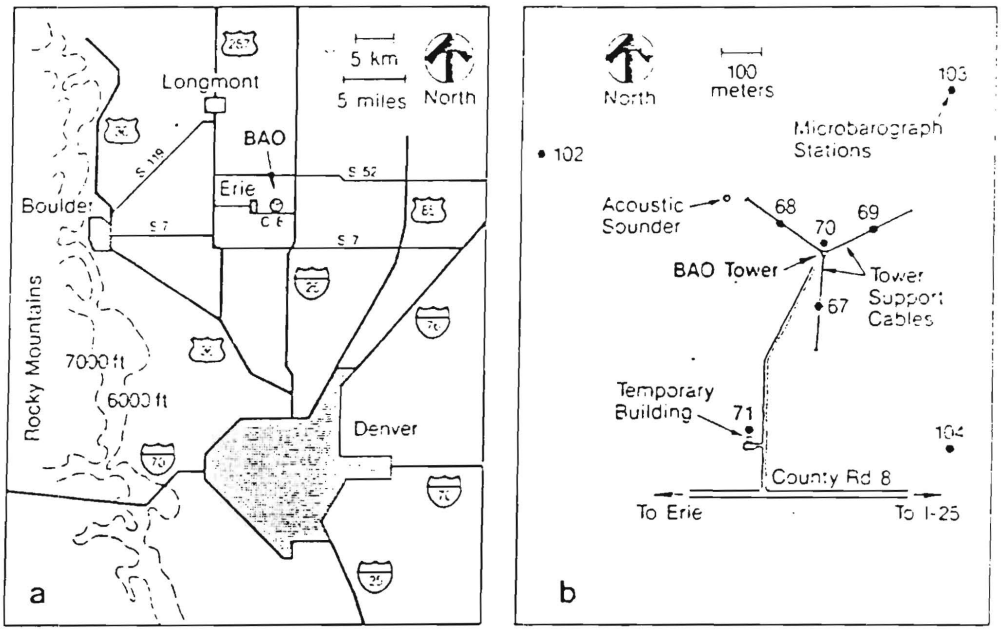
Longmont
5 km
5 miles
North
BAO
Erie
Boulder
Rocky Mountains
7000 ft
6000 ft
Denver
a
North
100
meters
103
Microbarograph
Stations
102
Acoustic
Sounder
68
69
70
BAO Tower
Tower
Support
Cables
67
Temporary
Building
71
104
County Rd 8
To Erie
To I-25
b

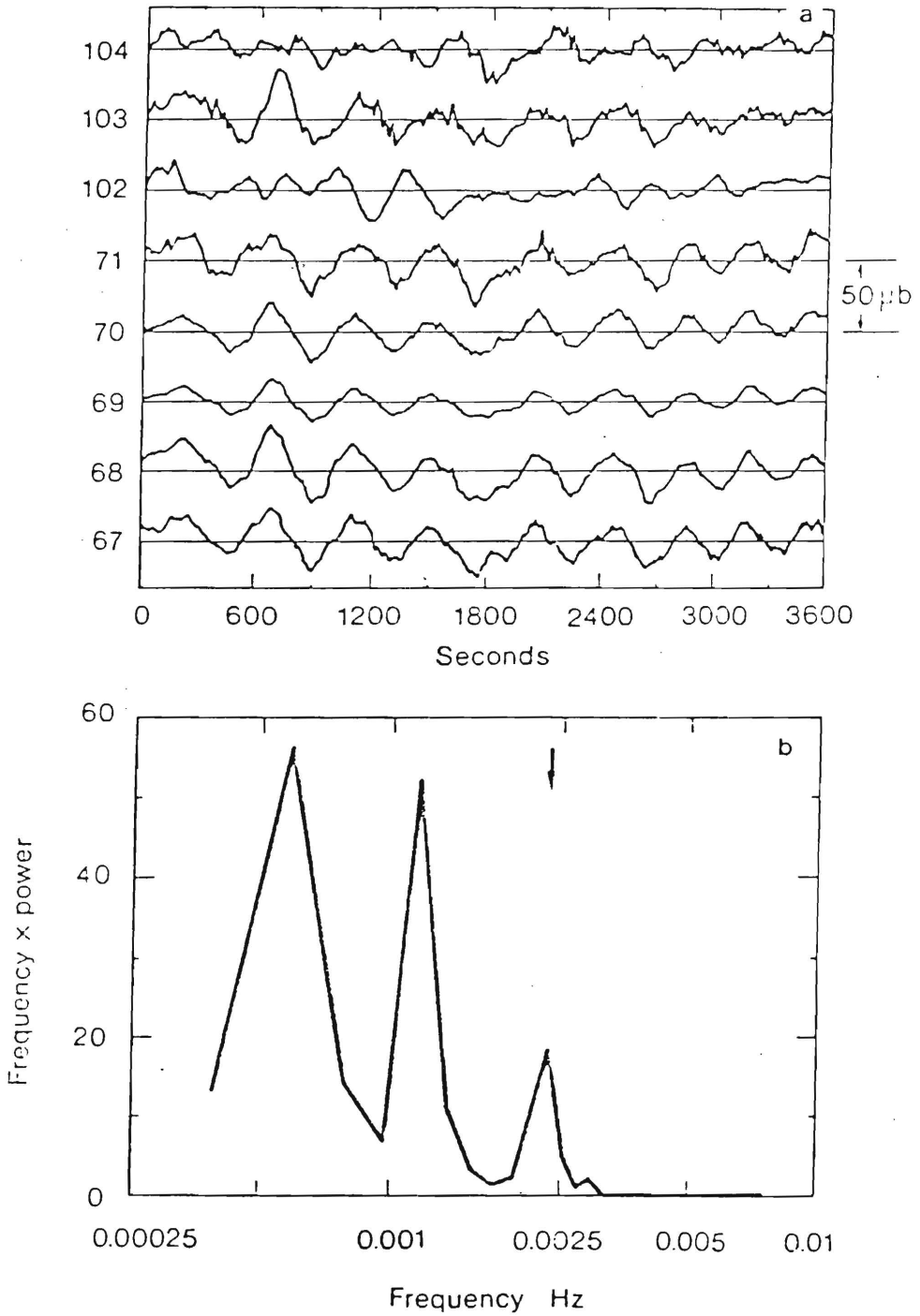
a
104
103
102
71
70
69
68
67
50 μb
0
600
1200
1800
2400
3000
3600
Seconds
b
60
40
20
0
Frequency x power
0.00025
0.001
0.0025
0.005
0.01
Frequency Hz

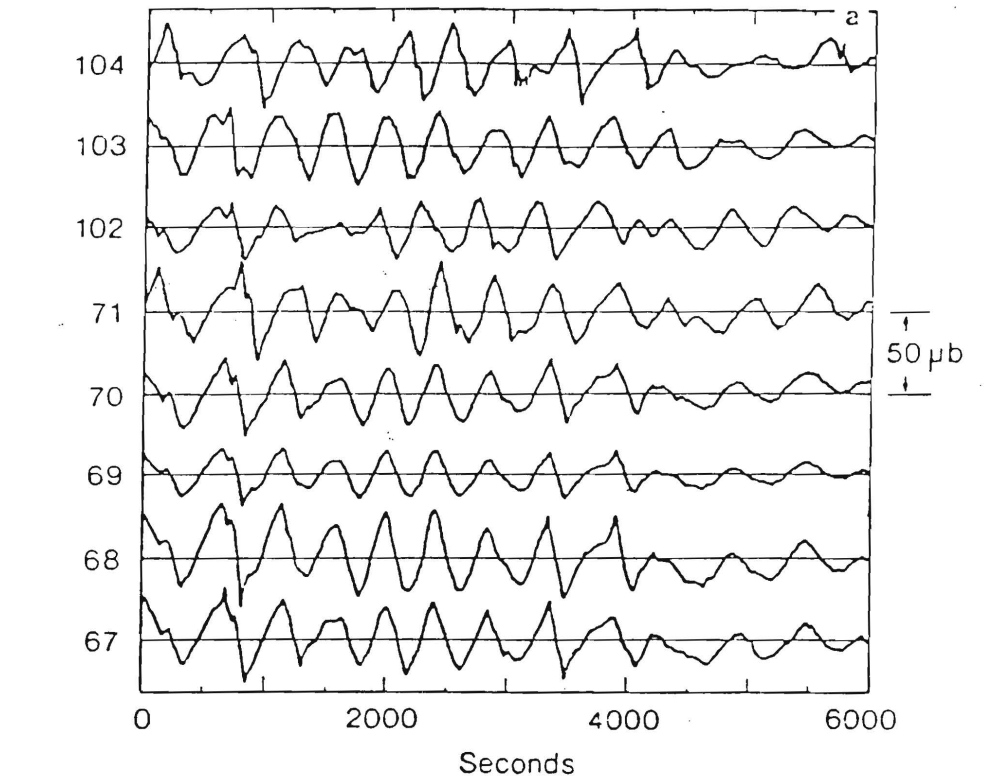
a
104
103
102
71
70
69
68
67
50 µb
0
2000
4000
6000
Seconds

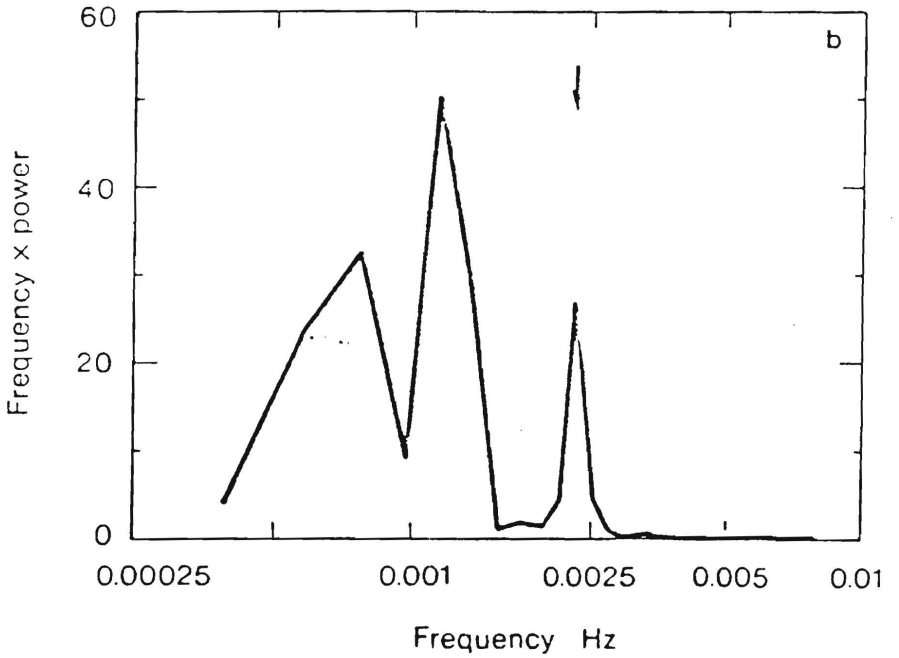
b
60
40
20
0
Frequency x power
0.00025
0.001
0.0025
0.005
0.01
Frequency Hz

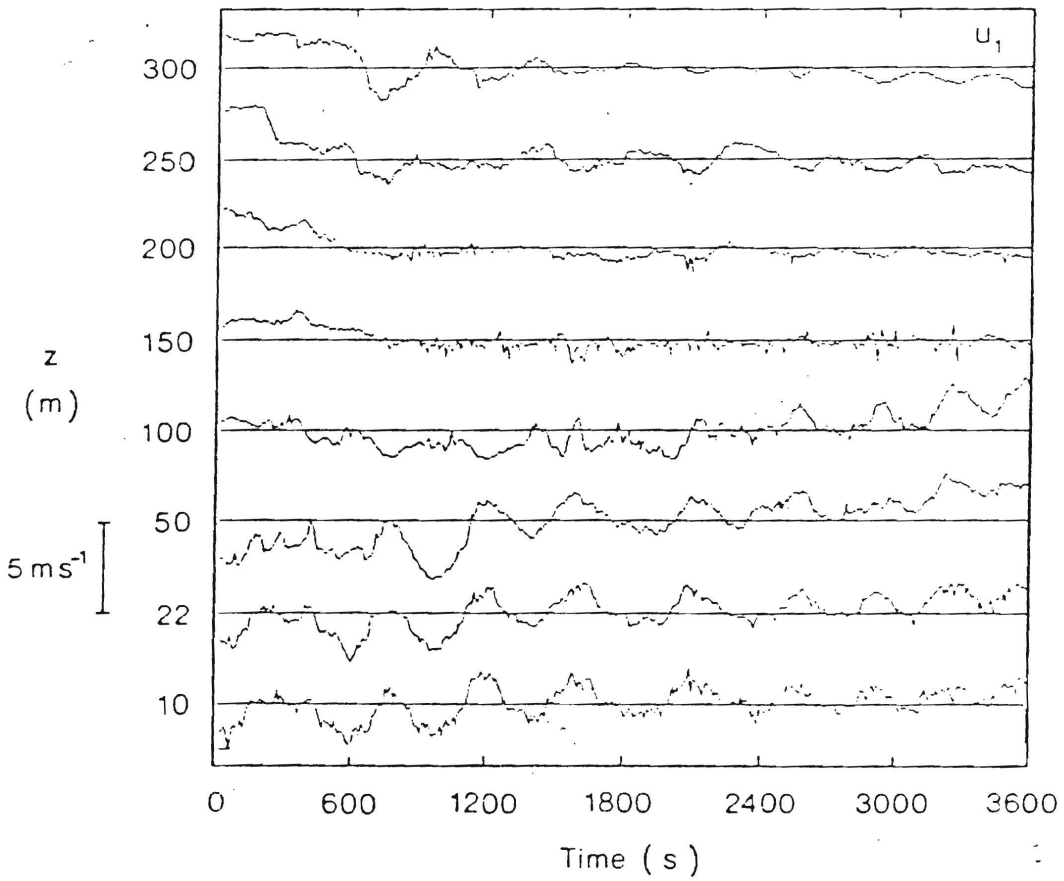
u_1
300
250
200
150
100
50
22
10
z
(m)
5 m s^{-1}
0
600
1200
1800
2400
3000
3600
Time (s)

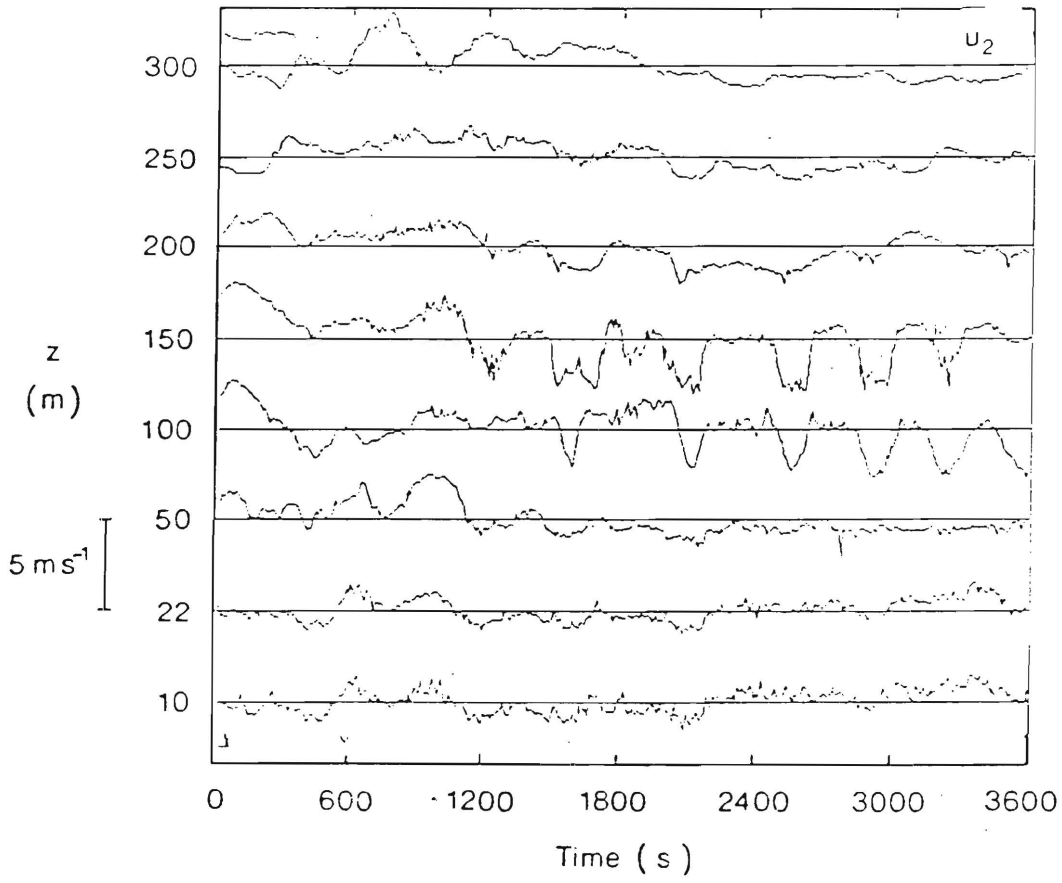
u_2
300
250
200
150
100
50
22
10
z
(m)
5 m s^{-1}
0
600
1200
1800
2400
3000
3600
Time (s)

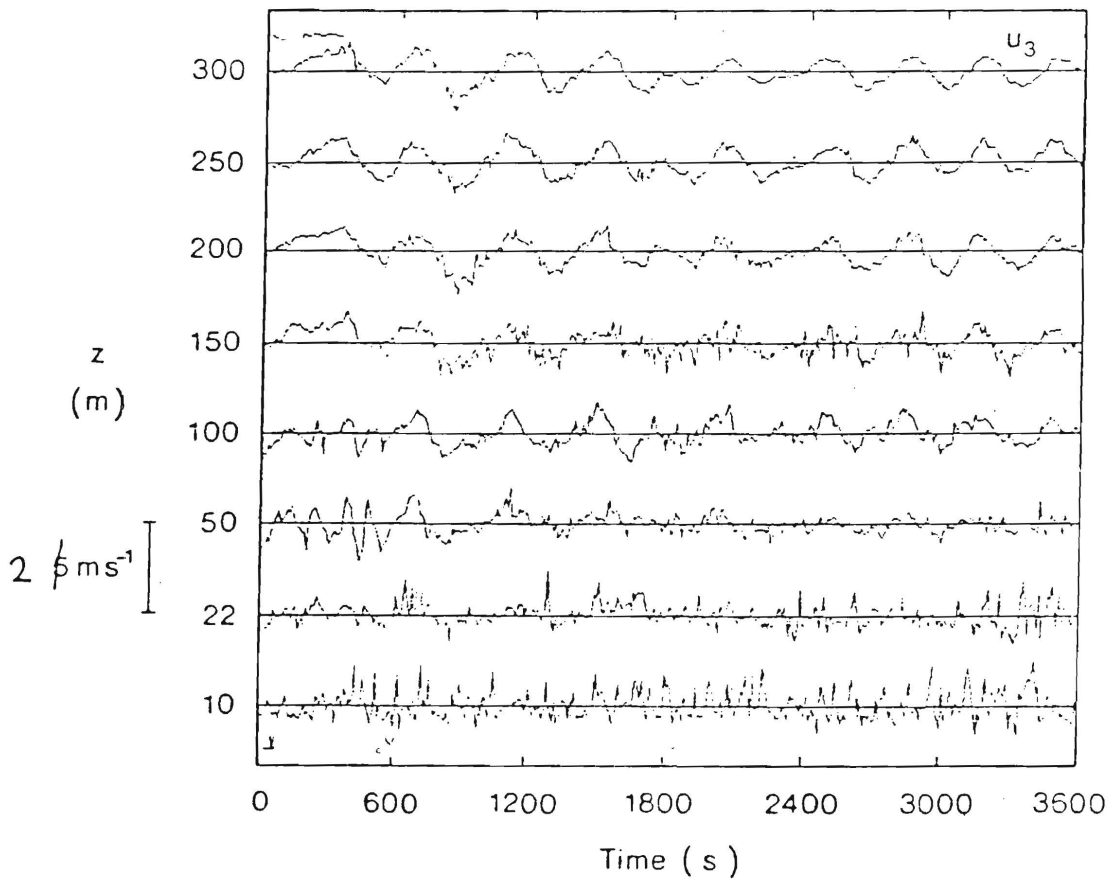
u_3
300
250
200
150
100
50
22
10
z
(m)
2 ms^{-1}
0
600
1200
1800
2400
3000
3600
Time (s)

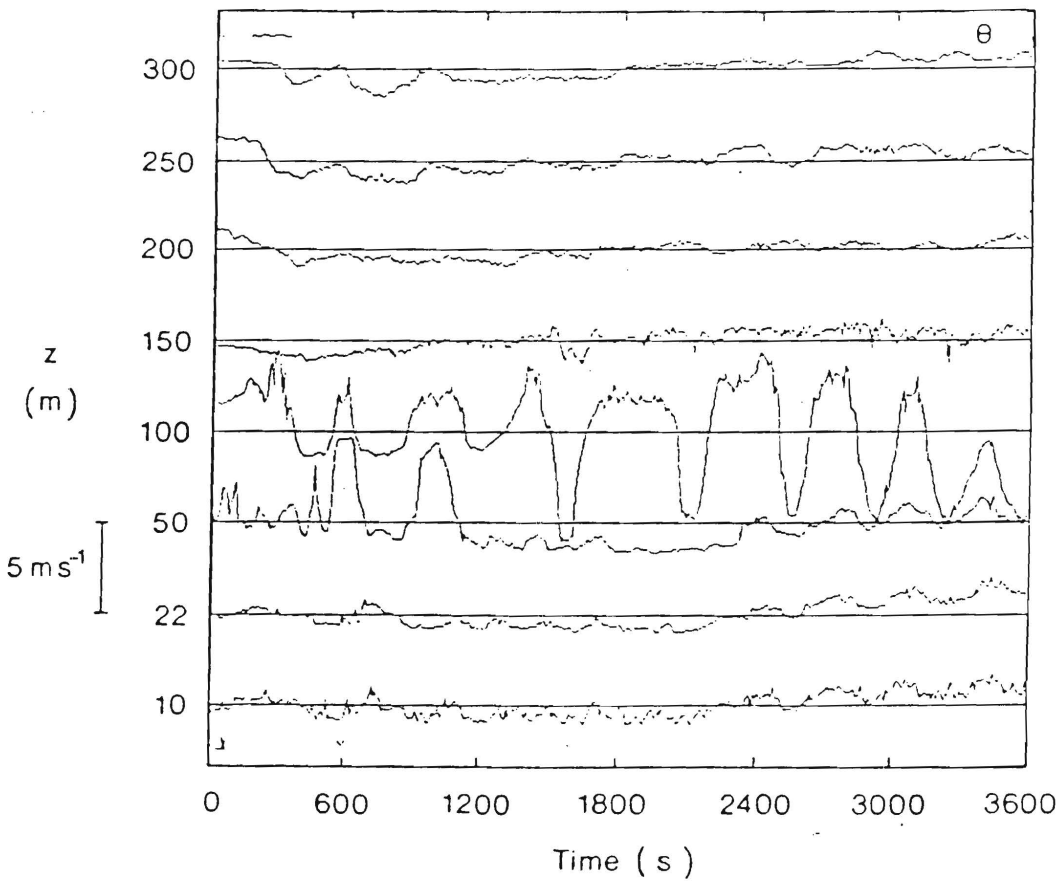
θ
300
250
200
150
100
50
22
10
z
(m)
5 m s⁻¹
0
600
1200
1800
2400
3000
3600
Time (s)

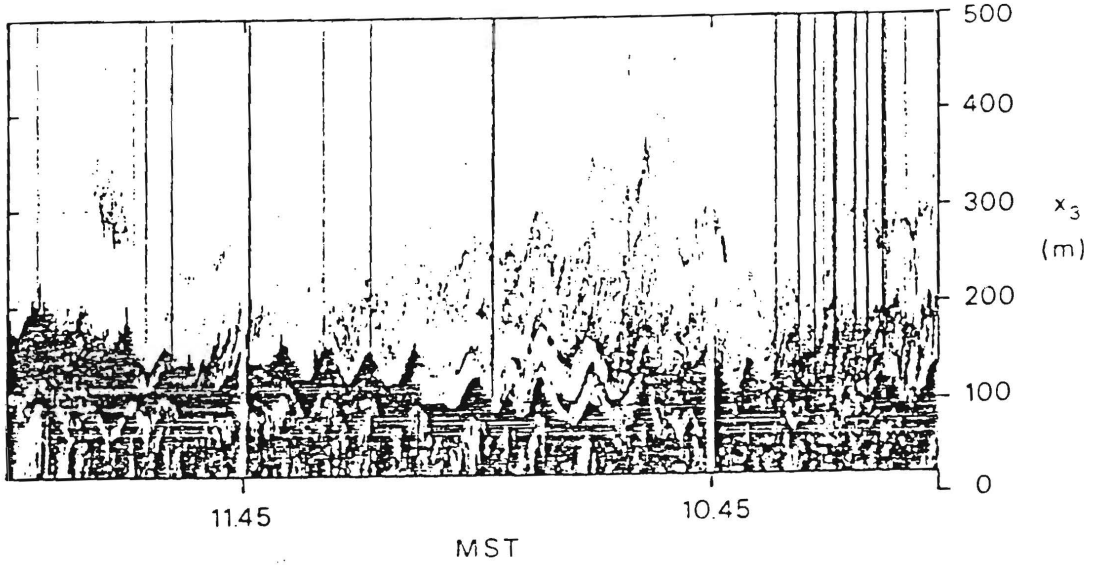
500
400
300
200
100
0
x_3
(m)
11.45
10.45
MST

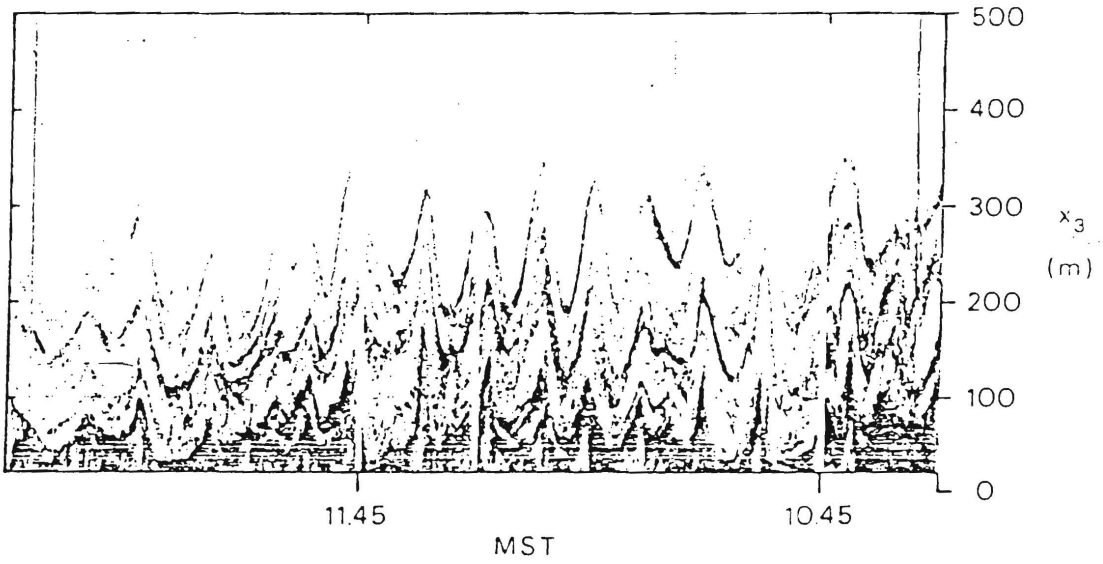
500
400
300
200
100
0
x_3
(m)
11.45
10.45
MST

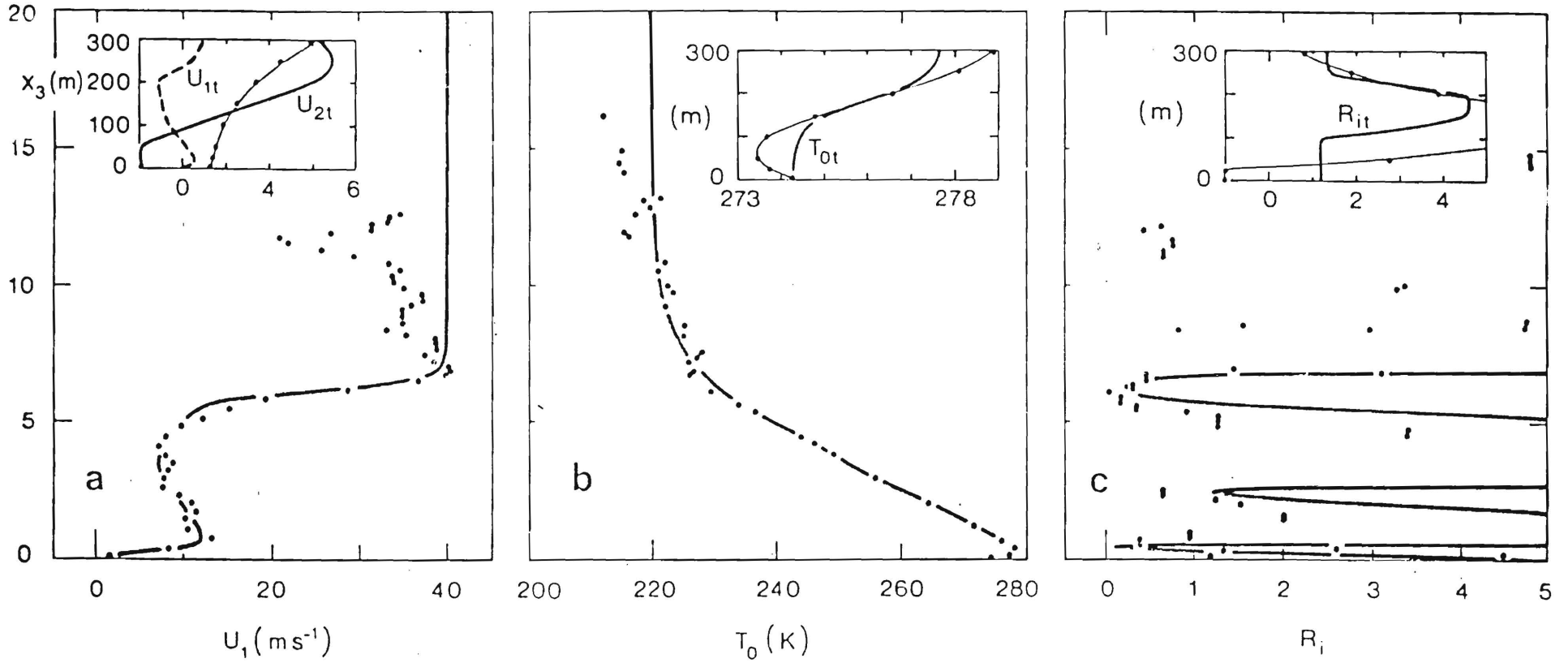
20
15
10
5
0
x_3 (m)
300
200
100
0
U_{1t}
U_{2t}
0
4
6
a
0
20
40
U_1 (m s^{-1})
300
(m)
0
T_{0t}
273
278
b
200
220
240
260
280
T_0 (K)
300
(m)
0
R_{it}
0
2
4
c
0
1
2
3
4
5
R_i

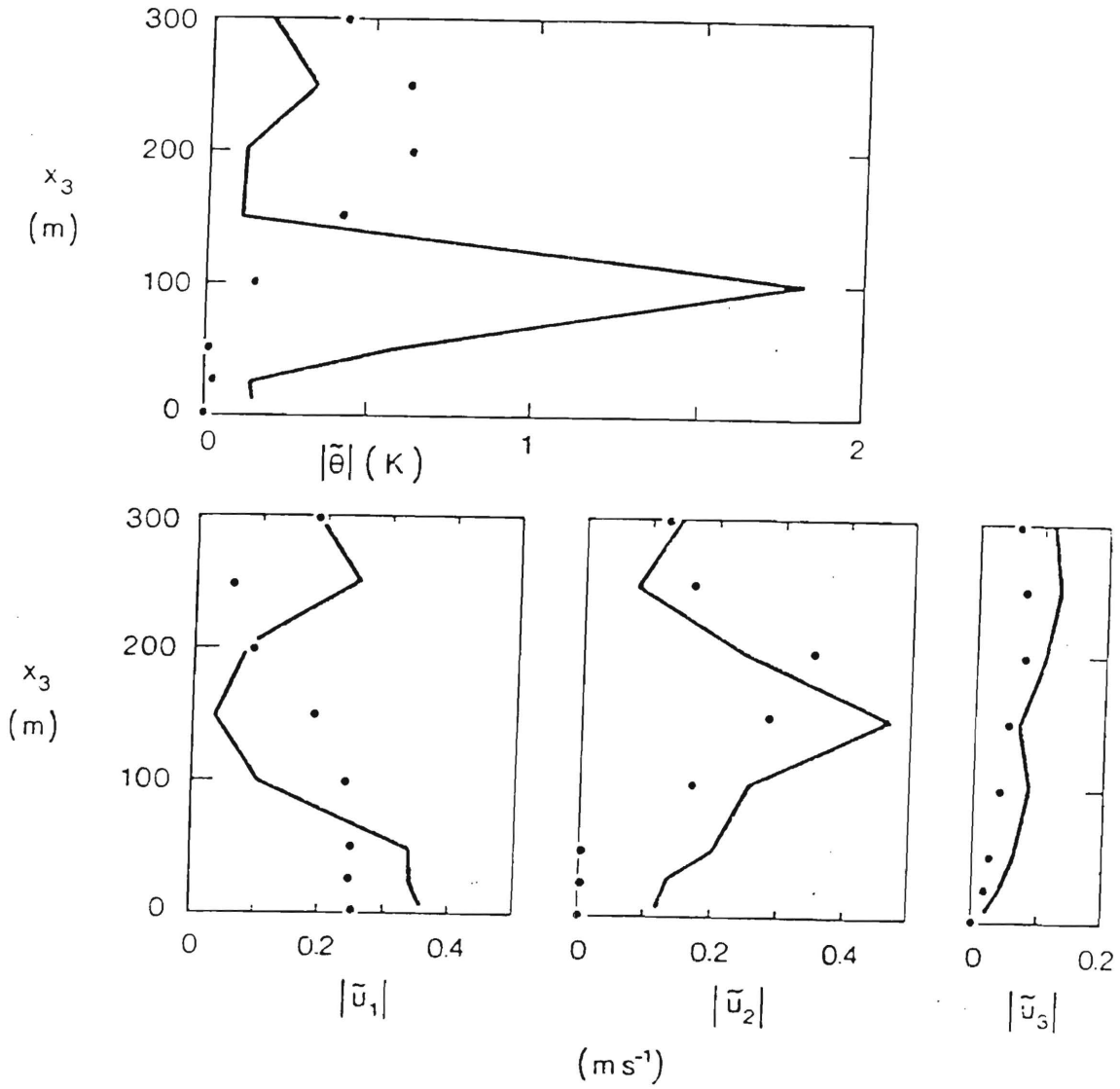
300
200
100
0
x_3
(m)
0
1
2
$|\tilde{\theta}|$ (K)
0
0.2
0.4
$|\tilde{u}_1|$
$|\tilde{u}_2|$
$|\tilde{u}_3|$
(m s^{-1})

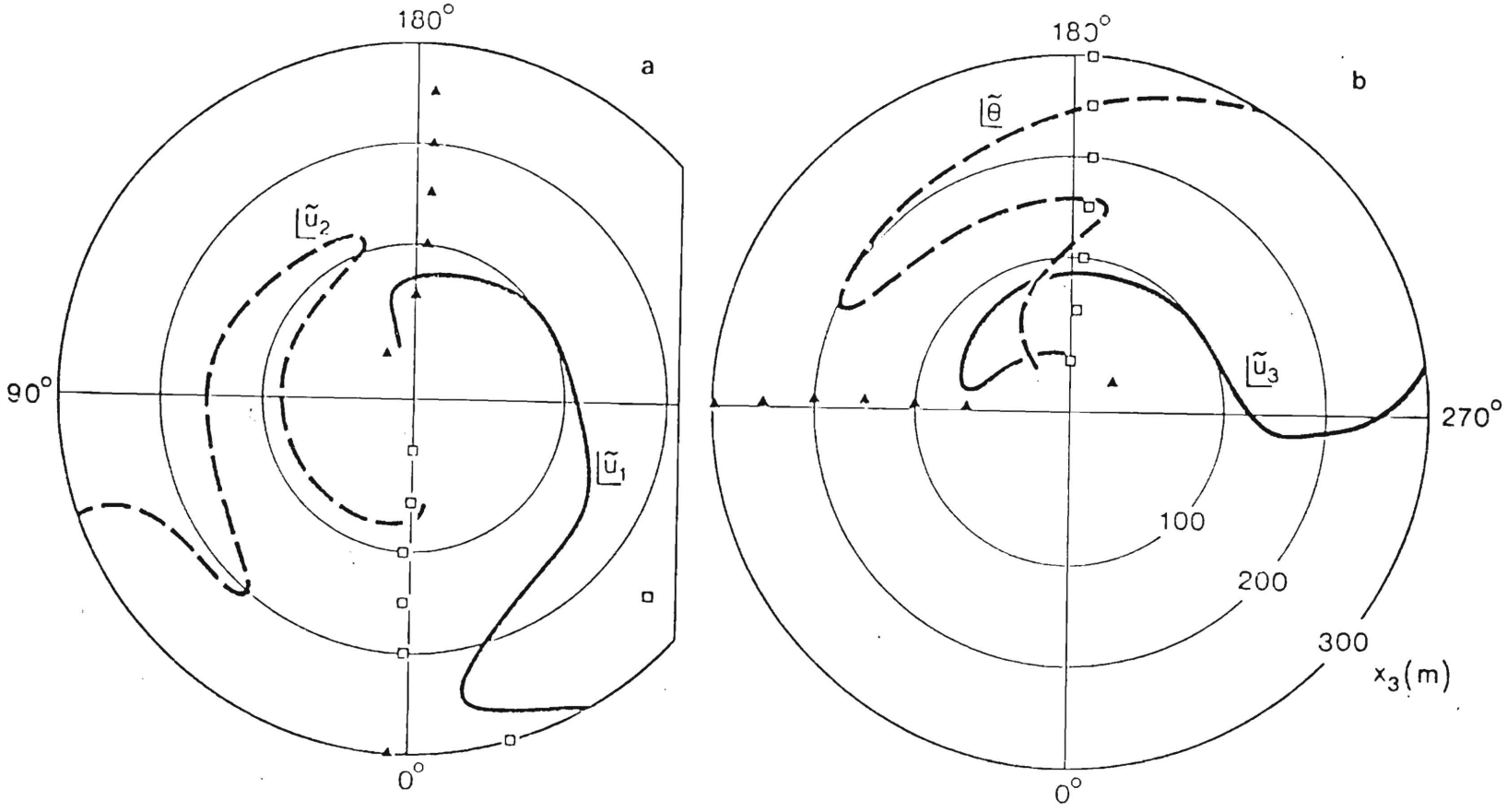
180°
a
90°
$\tilde{u}_2$
$\tilde{u}_1$
0°
180°
b
$\tilde{\theta}$
$\tilde{u}_3$
270°
100
200
300
x_3(m)
0°

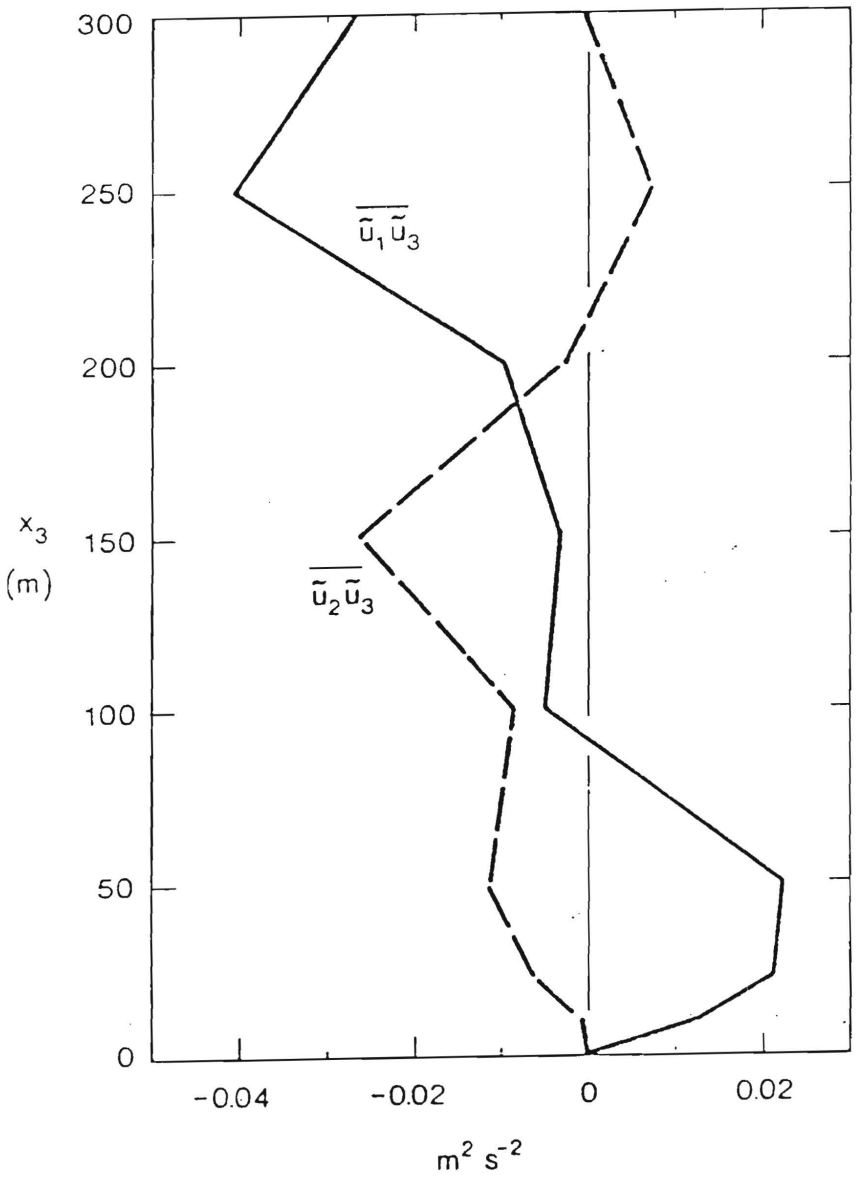
300
250
200
150
100
50
0
x_3
(m)
$\overline{\tilde{u}_1\tilde{u}_3}$
$\overline{\tilde{u}_2\tilde{u}_3}$
-0.04
-0.02
0
0.02
$m^2\ s^{-2}$

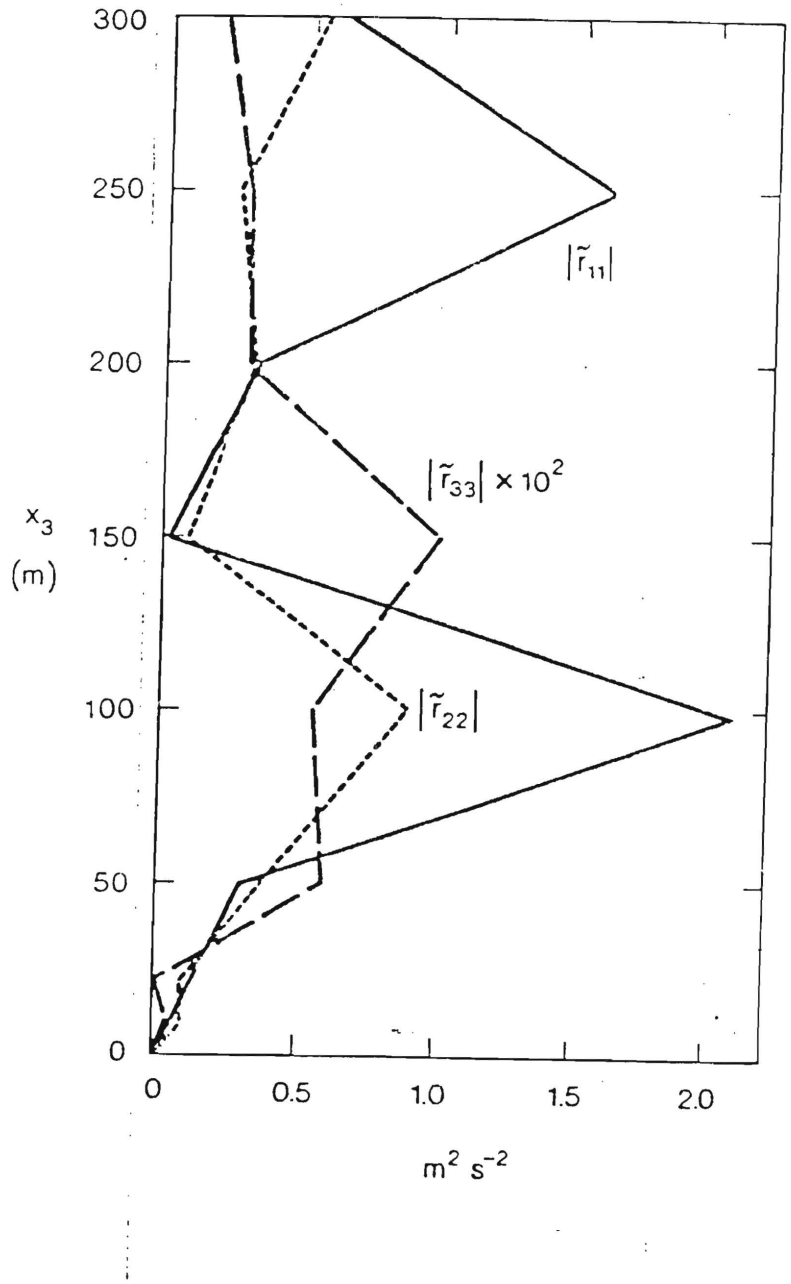
300
250
200
150
100
50
0
x_3
(m)
$|\tilde{r}_{11}|$
$|\tilde{r}_{33}| \times 10^2$
$|\tilde{r}_{22}|$
0
0.5
1.0
1.5
2.0
$m^2\ s^{-2}$

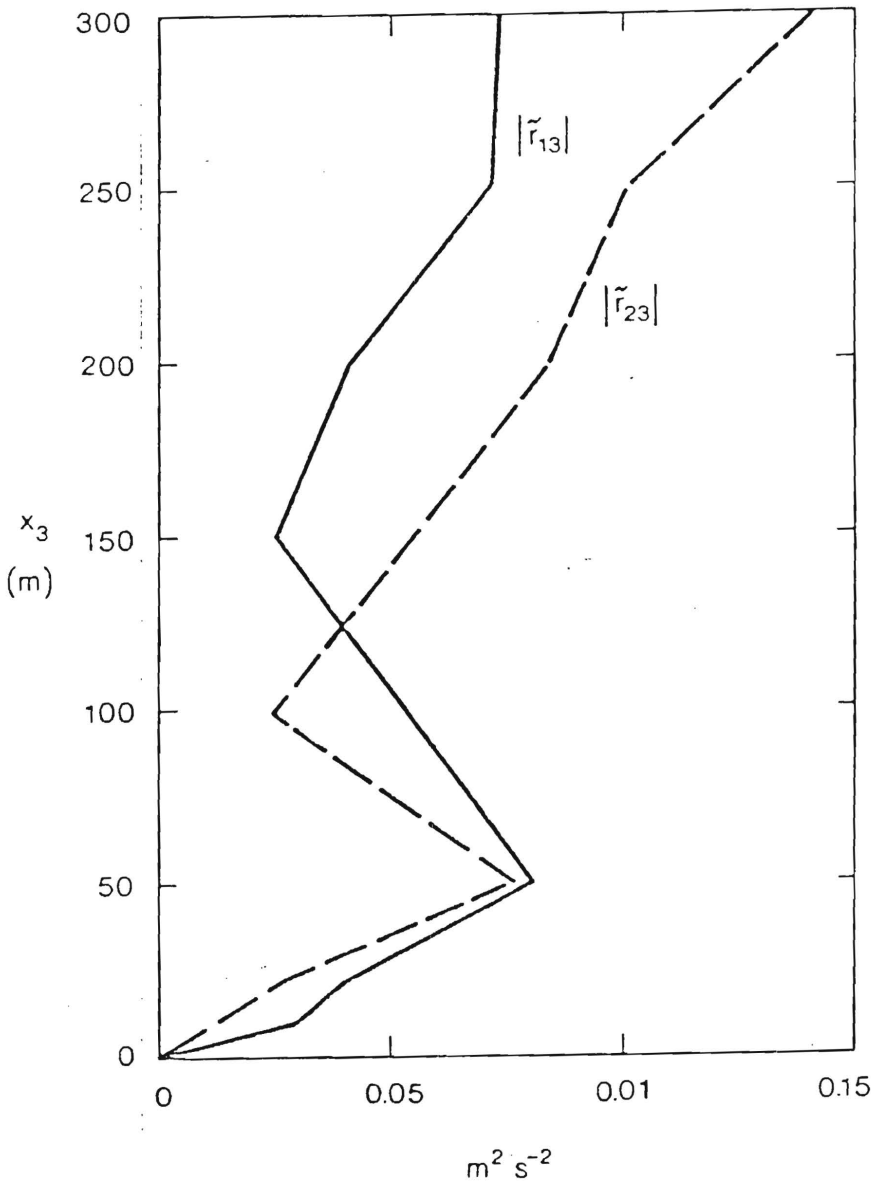
300
250
200
150
100
50
0
x_3
(m)
$|\tilde{r}_{13}|$
$|\tilde{r}_{23}|$
0
0.05
0.01
0.15
$m^2\ s^{-2}$

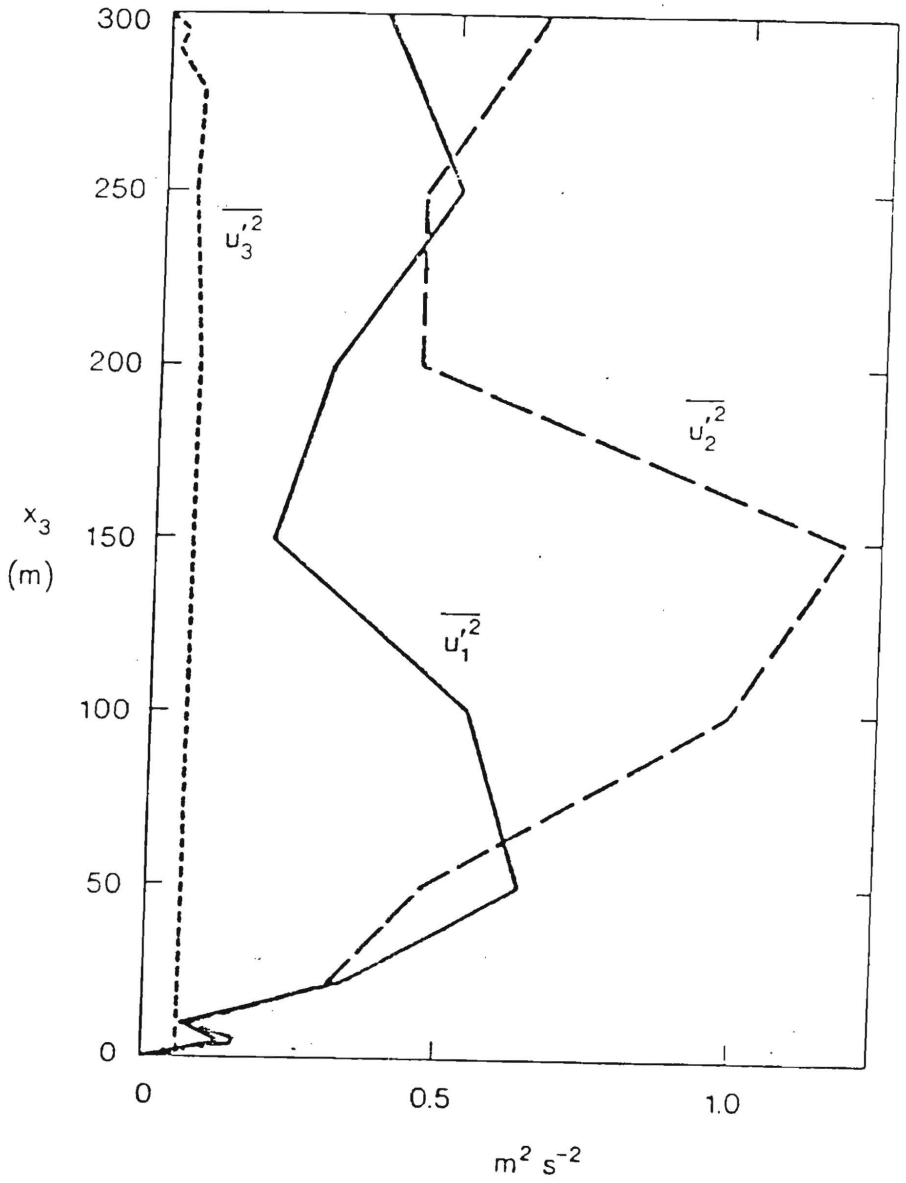
300
250
200
150
100
50
0
x_3
(m)
$\overline{u_3'^2}$
$\overline{u_2'^2}$
$\overline{u_1'^2}$
0
0.5
1.0
$m^2\ s^{-2}$

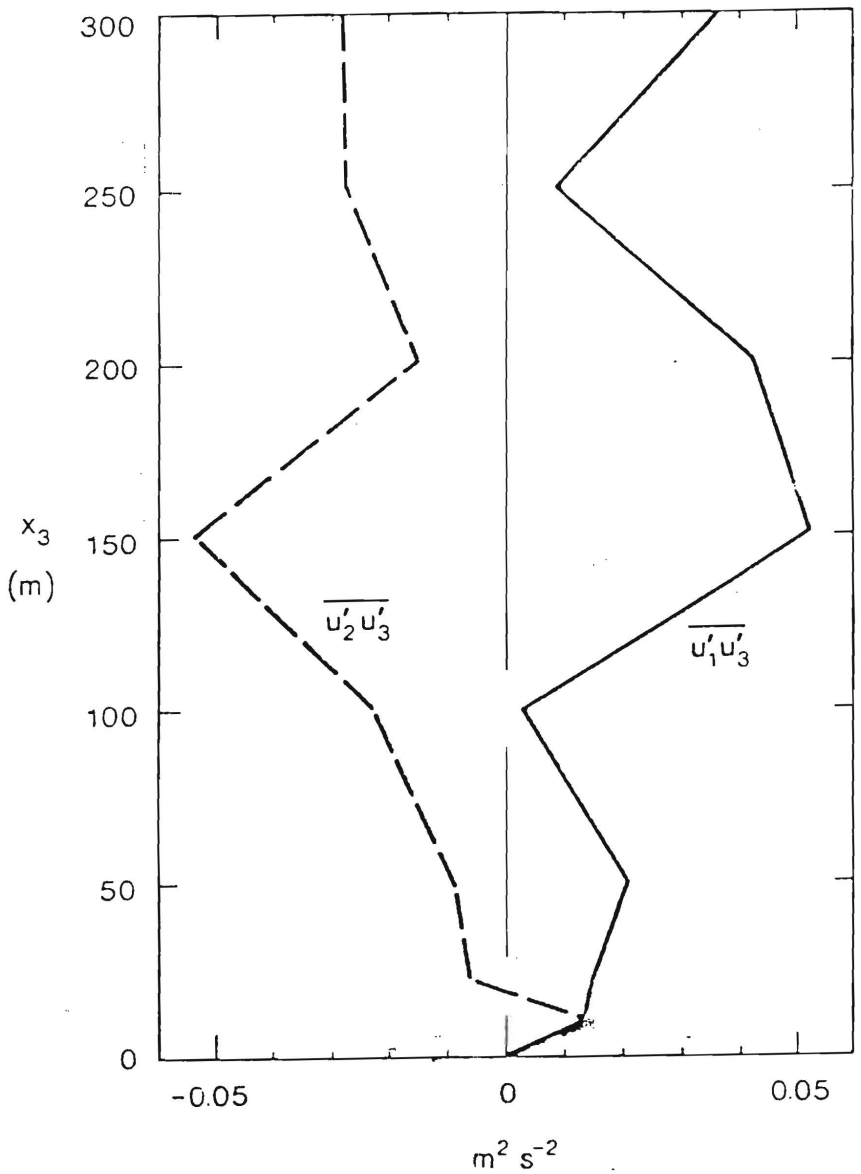
300
250
200
150
100
50
0
x_3
(m)
$\overline{u_2' u_3'}$
$\overline{u_1' u_3'}$
-0.05
0
0.05
$m^2 s^{-2}$

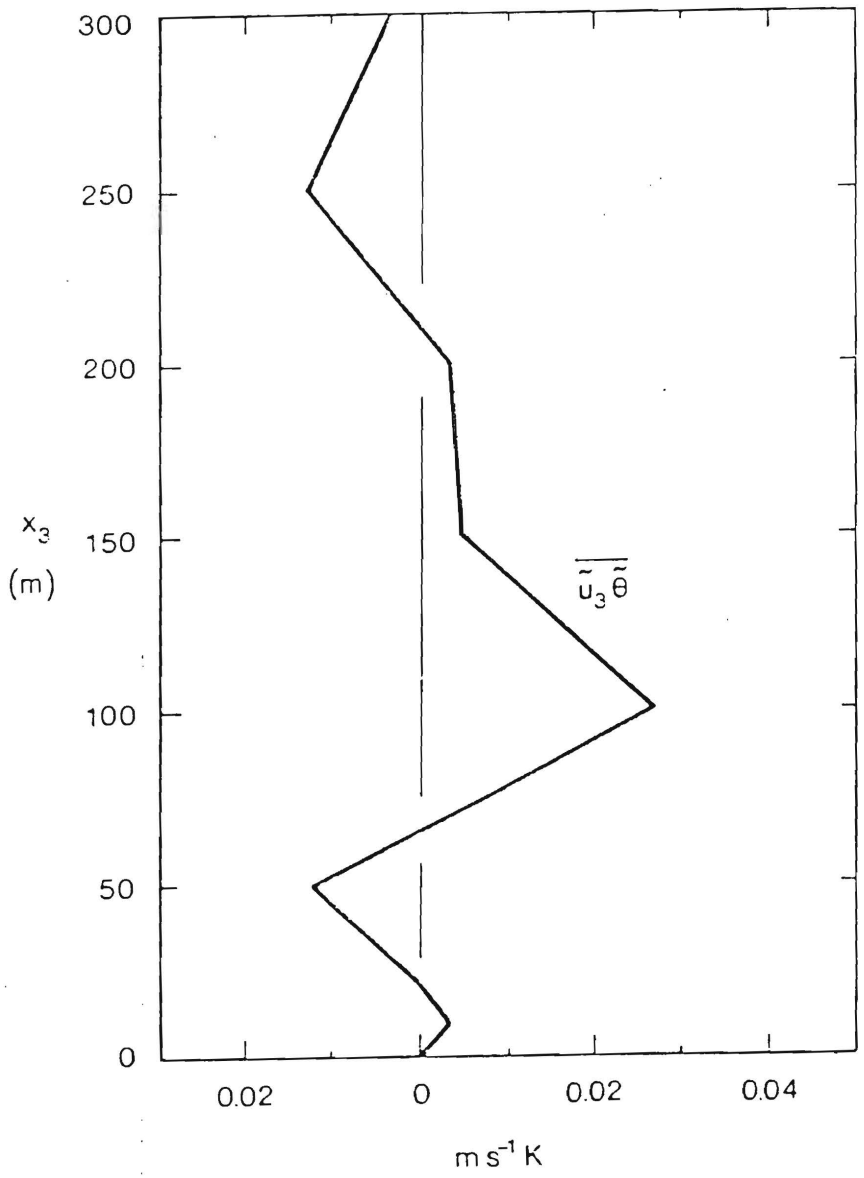
300
250
200
150
100
50
0
x_3
(m)
$\overline{\tilde{u}_3\tilde{\theta}}$
0.02
0
0.02
0.04
m s^{-1} K

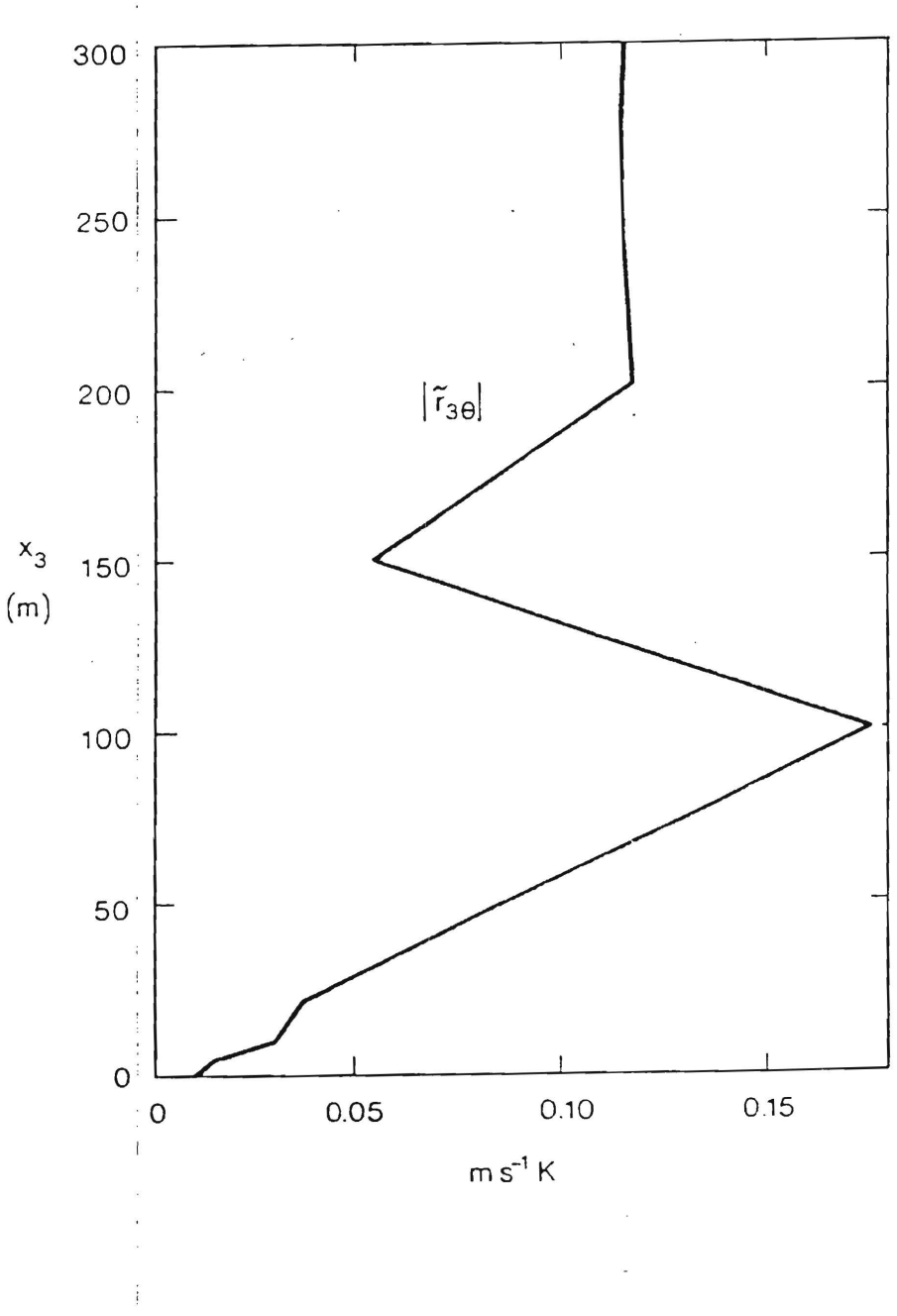
300
250
200
150
100
50
0
x_3
(m)
$|\tilde{r}_{3\theta}|$
0
0.05
0.10
0.15
m s^{-1} K

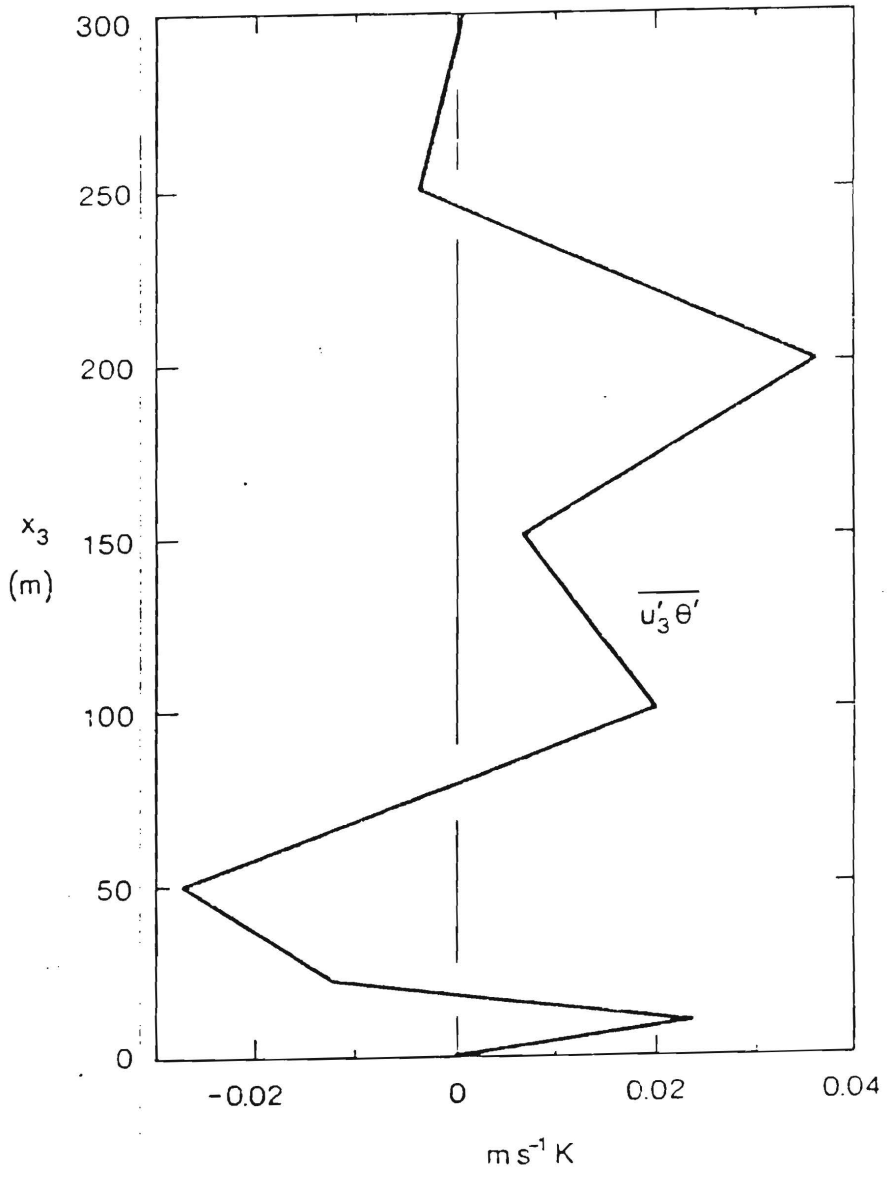
300
250
200
150
100
50
0
x_3
(m)
$\overline{u_3'\theta'}$
-0.02
0
0.02
0.04
m s^{-1} K

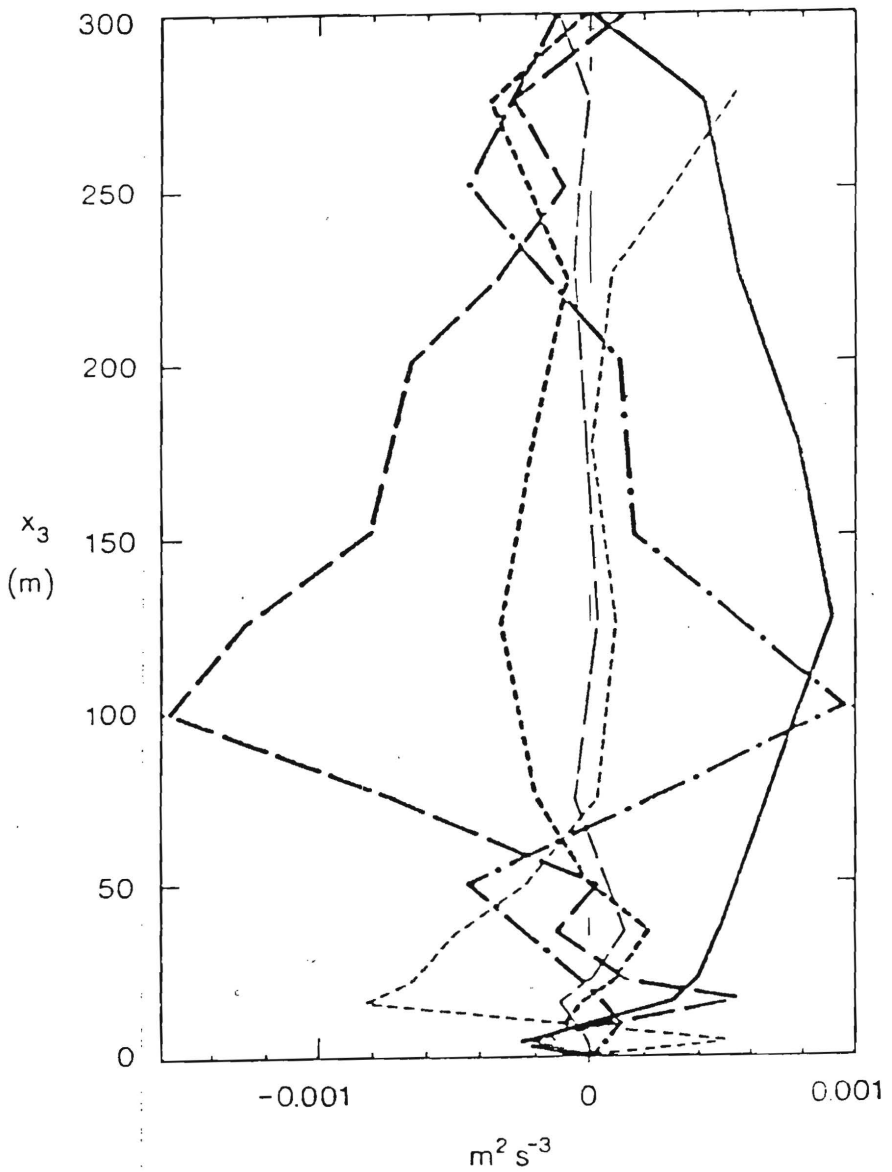
300
250
200
150
100
50
0
x_3
(m)
-0.001
0
0.001
$m^2 s^{-3}$

90°
0°
180°
Φ_{13}
a
Φ_{23}
0°
180°
270°
0
100
200
300
x_3 (m)
b

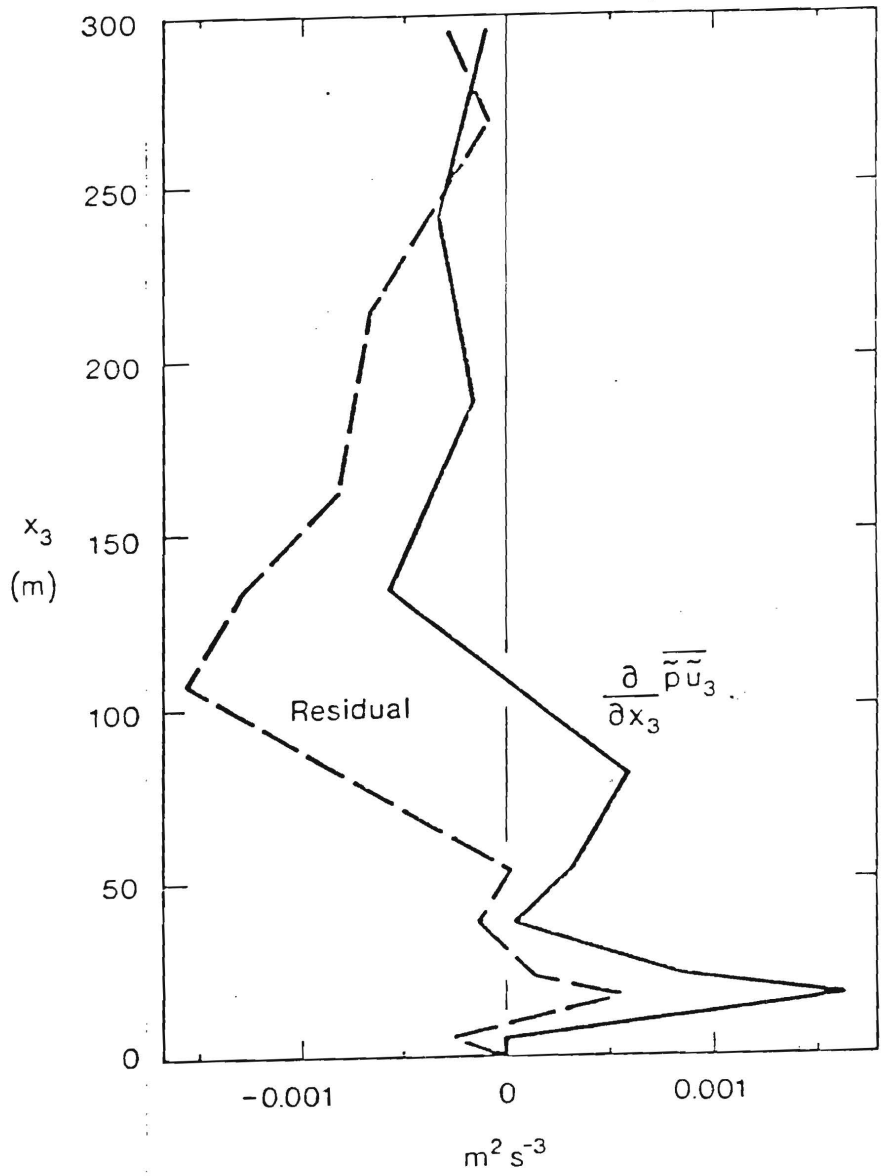
300
250
200
150
100
50
0
x_3
(m)
Residual
$\frac{\partial}{\partial x_3}\overline{\tilde{\rho}\tilde{u}_3}$
-0.001
0
0.001
$m^2 s^{-3}$

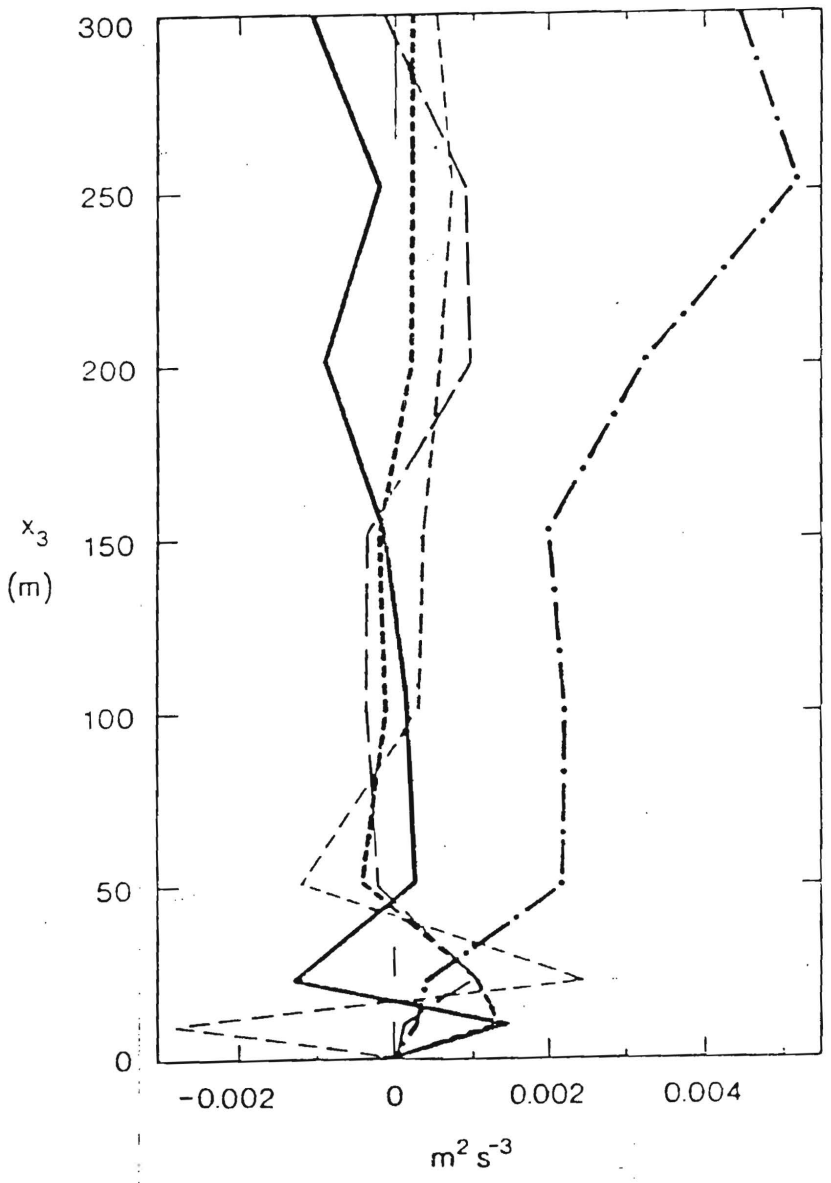
300
250
200
150
100
50
0
x_3
(m)
-0.002
0
0.002
0.004
$m^2 s^{-3}$

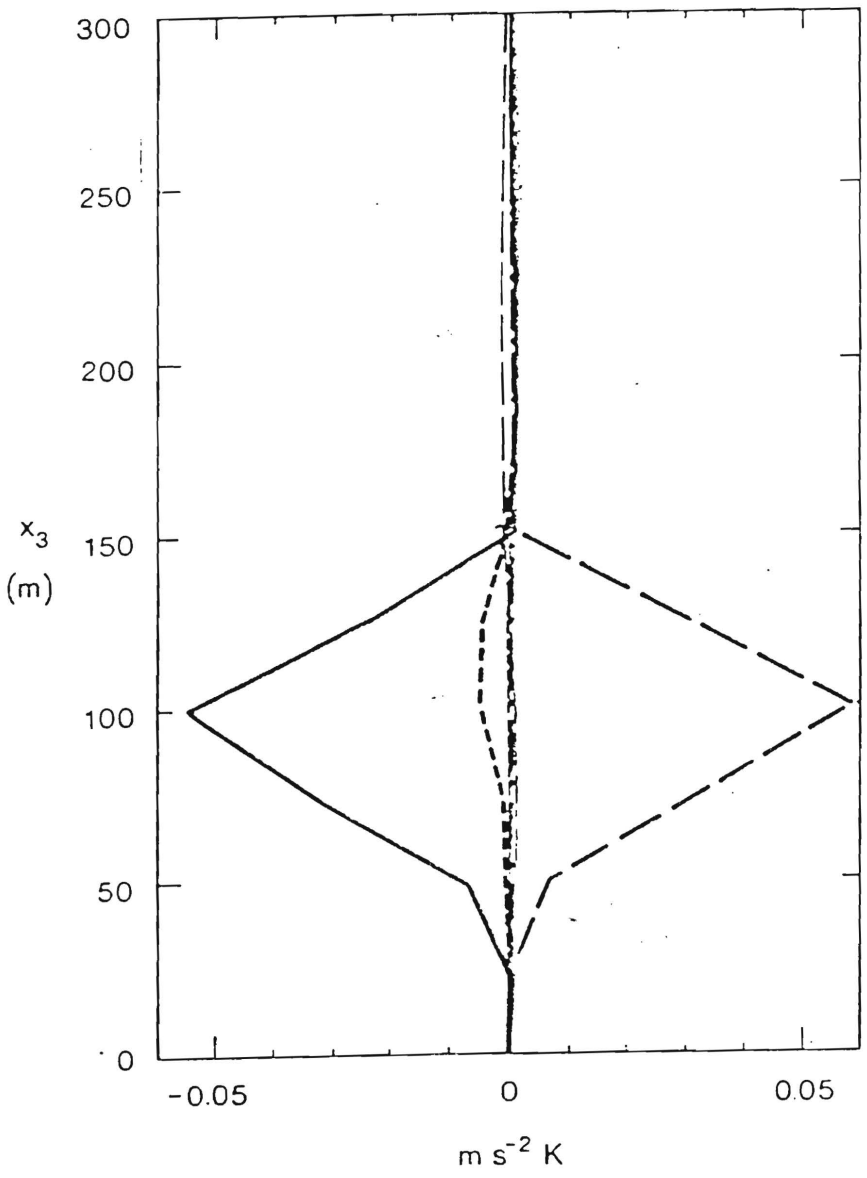
300
250
200
150
100
50
0
x_3
(m)
-0.05
0
0.05
m s^{-2} K

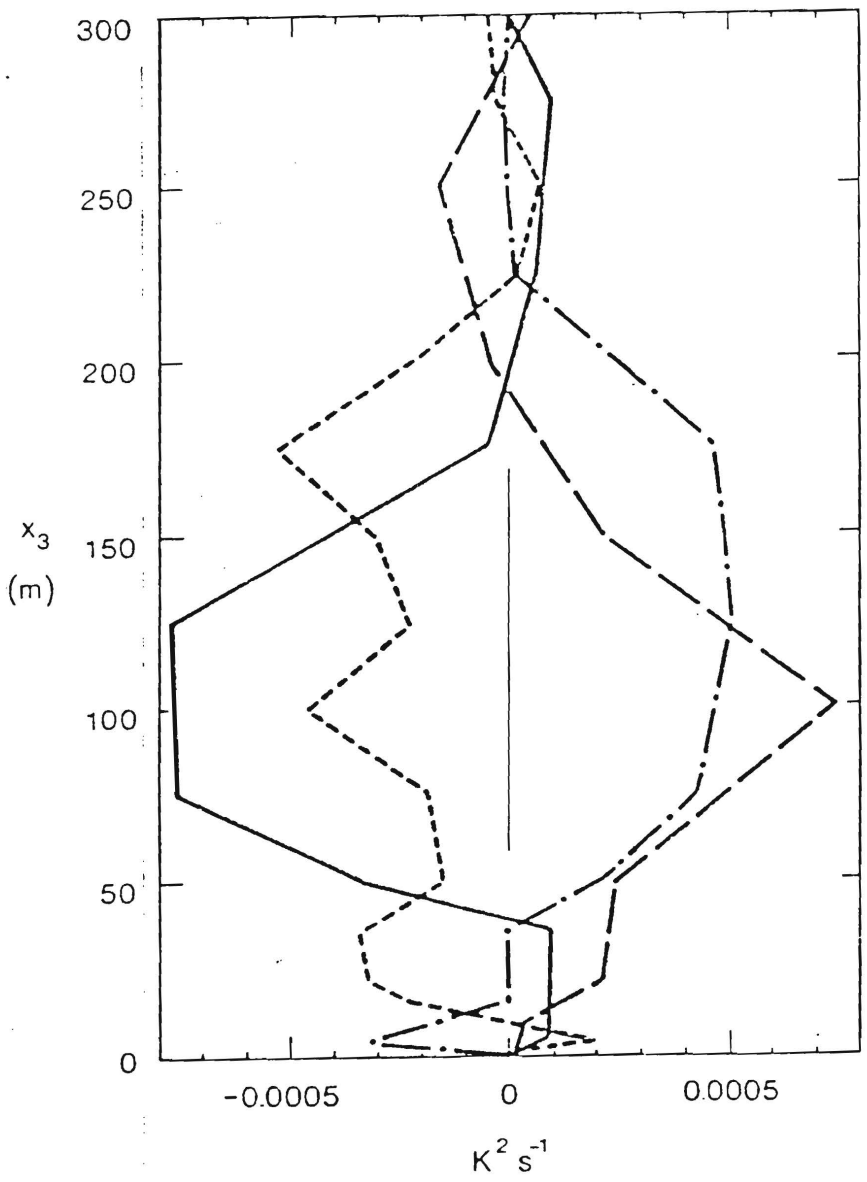
300
250
200
150
100
50
0
x_3
(m)
-0.0005
0
0.0005
$K^2 s^{-1}$

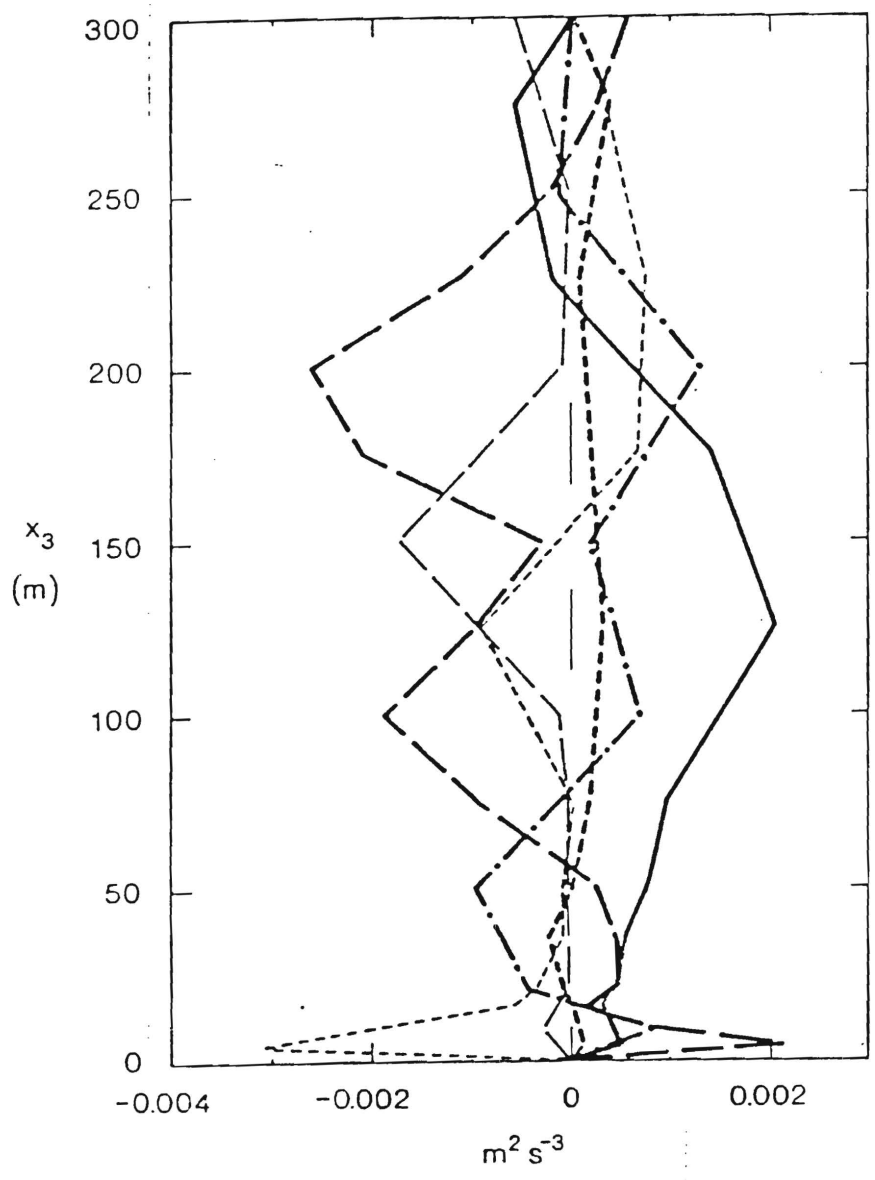
300
250
200
150
100
50
0
x_3
(m)
-0.004
-0.002
0
0.002
$m^2 s^{-3}$